Towards Sequential Design for Multi-Period Repetitive Control with Application to a Wide-Format Industrial Printer

Bevers, P.P.F.

Award date:
2018

Towards Sequential Design for Multi-Period Repetitive Control: with Application to a Wide-Format Industrial Printer

Master of Science Thesis

Author
P.P.F. Bevers MSc 0858003

Research Group and Department
Control Systems Technology - Mechanical Engineering

Master Program
Systems & Control

Supervisors:
ir. L.L.G. Blanken
dr.ir. F.A.J. Boeren
dr.ir. S.H. Koekebakker
dr.ir. T.A.E. Oomen

CST 2018.107

Eindhoven, December 4, 2018

Master of Science Thesis

Committee: dr.ir. T.A.E. Oomen ‡
dr.ir. G. Witvoet ‡
dr.ir. S.H. Koekebakker ∗
dr. A.Y. Pogromskiy ⋆
ir. L.L.G. Blanken ‡

‡ Eindhoven University of Technology
Department of Mechanical Engineering
Control System Technology

⋆ Eindhoven University of Technology
Department of Mechanical Engineering
Dynamics and Control

∗ Océ Technologies B.V.
Research and Development

Abstract

The digital graphical art printing market is rapidly developing, where wide-format Roll-To-Roll (RTR) printing systems play an important role. To be competitive in this market, high production speed, high product qualities, and large medium versatility are important requirements. A key factor in printing process is the positioning of the print heads with respect to the medium. However, positioning accuracy and speed are limited by so-called Medium Positioning Errors (MPEs) arising from step-wise medium transpositions after each print-pass. These errors cause misalignment of consecutive print-passes, which negatively affects the print quality. There are several sources contributing to MPEs, such as rotating elements, which results in multiple dominant periodic components. These periodic errors need to be compensated to achieve the required positioning performance.

There are several approaches which can be taken to reduce the effects of MPEs. Pre-existing approaches aim to i) reduce MPEs through improved redesign of the media handling, which is typically expensive due to the required hardware components, or ii) conceal MPEs by using multiple overlapping print-passes, which comes at the cost of production speed. A potential alternative to these approaches is to reduce MPEs through active position control of the medium or print heads. Typical control approaches, such as feedback control and feedforward control, cannot be applied, since the MPEs are not available in real-time. Instead, the MPE measurements become available after a print-pass due to scanning and image processing. Hence, their periodicity can be exploited through batch-wise learning control. Iterative Learning Control (ILC) shows promising results on a wide-format printing system, however Repetitive Control (RC) is more suited for handling continuously repeating disturbances. A repetitive controller enables to accurately reject periodic disturbances. To reject multiple periodic components in MPEs, in this research it is investigated to combine multiple repetitive controllers in parallel or in so-called cascaded structure, i.e., multi-period RC. Although these frameworks exist in literature, existing design procedures yield conservative results which severely limit performance.

The aim of this thesis is to compensate for periodically recurring medium positioning errors by developing a multi-period RC sequential design framework, that achieves high positioning accuracy and increased productivity.

In multi-period RC, multiple repetitive controllers are connected in closed-loop, indicating that interactions between the controllers are unavoidable. However, analysis of the resulting closed-loop system for multi-period RC reveals the potential for sequentially designing the individual repetitive controllers. In this way, each individual repetitive controller explicitly accounts for these interactions in the design. Often in practice the interactions can be accurately measured, due to accurate Frequency Response Function (FRF) measurements. An explicit sequential design procedure is developed in this research and validated on a wide-format RTR printing system. It is confirmed that the approach results in less conservative designs in comparison with existing design methods, and improves performance.

Experimental results on a wide-format RTR printing system demonstrate the potential of multi-period RC for rejection of disturbances with multiple unrelated periods. Through sequential design of multiple cascaded repetitive controllers, fast learning behavior and high positioning performance is achieved. These results confirm the benefits of the developed approach, and illustrate its potential for increased printing quality and production speed in industrial printing systems.

Acknowledgements

First of all, I would like to thank my coaches Frank Boeren, Lennart Blanken, and Sjirk Koekebakker. I am very grateful for their guidance and fruitful discussions during my graduation. Their knowledge and practical experience helped me to understand things and get new insights. Further, I would like to thank Tom Oomen and Gert Witvoet for their coaching and further contributions during my master *System and Control - Control Systems Technology*. I also would like to thank Océ Technologies B.V. for providing me the opportunity to perform my graduation research at this company. Thanks to all my colleagues at Océ Technologies B.V. for the fine cooperation. Finally, I would like to thank my family and friends, since they are always there for me.

Contents

Nomenclature

Greek Symbols

α	Learning gain	
Γ	Nyquist contour	
ω	Frequency	[rad/s]

Latin Symbols

f	Frequency	[Hz]
f_c	Cut-off frequency	[Hz]
f_d	Disturbance frequency	[Hz]
f_s	Sample frequency	[Hz]
k	Discrete-time instant	
j	Imaginary unit	
N	Period length in number of samples	
n	Number of repetitive controllers	
n_L	Unit delays of the learning filter	
n_Q	Unit delays of the robustness filter	
t	Time	[s]
T_s	Sample time	[s]

Sets

$\mathbb{C}$	Complex numbers
$\mathbb{D}$	Open unit disc, i.e., $\{z \in \mathbb{C}, \lvert z\rvert < 1\}$
$\mathbb{E}$	Extension of unit disc, i.e., $\{z \in \mathbb{C}, \lvert z\rvert > 1\}$
$\mathbb{N}$	Set of natural numbers
$\mathbb{Q}$	Set of rational numbers
$\mathbb{R}$	Set of real numbers
$\mathbb{T}$	Unit circle $\{z \in \mathbb{C}, \lvert z\rvert = 1\}$
$\mathbb{Z}$	Set of integers

Mathematical Symbols

$\mathcal{RH}_\infty$	Set of proper, real rational transfer functions, with no poles in $\mathbb{T} \cup \mathbb{E}$.
$\mathcal{RL}_\infty$	Set of real rational transfer functions, with no poles in $\mathbb{T}$
$\mathcal{R}$	Set real rational transfer functions
$\mathcal{Z}$	Z-transform operator: $X(z) = \mathcal{Z}\{x(k)\} = \sum_{k=0}^{\infty} x(k) z^{-k}$

Acronyms

FIR	Finite Impulse Response
FRF	Frequency Response Function
ILC	Iterative Learning Control
IMP	Internal Model Principle
LCM	Least Common Multiple
LFT	Linear Fractional Transformation
LTI	Linear Time-Invariant
MIMO	Multiple-Input Multiple-Output
MPE	Medium Positioning Error
MPR	Medium Positioning Roll
PSD	Power Spectral Density
PSG	Periodic Signal Generator
RC	Repetitive Control
RTR	Roll-To-Roll
SISO	Single-Input Single-Output
ZOH	Zero-Order Hold
ZPETC	Zero Phase Error Tracking Control

Chapter 1

Introduction

1.1 Project Background: Industrial Wide-Format Roll-To-Roll Printing Systems

The printing system is an important factor in various industries, contributing from small scale printings to commercial banners, to store important documents or make large advertisements. The digital graphical art printing market is rapidly developing. Nowadays, wide-format Roll-To-Roll (RTR) printing systems, as depicted in Figure 1.1, play an important role in these markets. These wide-format RTR printing systems can continuously print various media up to a width of several meters, resulting in high production speed.

To keep up with industrial requirements, i.e., high production speed, product quality, and medium versatility, the printing systems have been developed into highly complex motion systems. The printing accuracy is up to micrometer level, to achieve high print qualities. However, the Medium Positioning Errors (MPEs) are important limitations to achieve these print qualities.

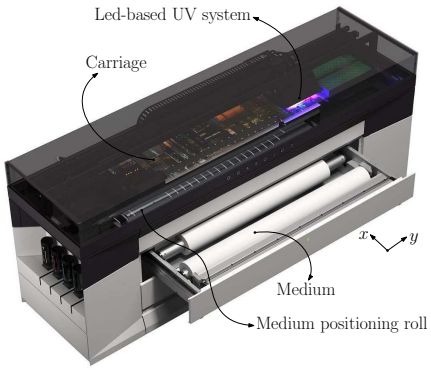

Figure 1.1: *Océ Colorado wide-format Roll-To-Roll (RTR) printing system.*

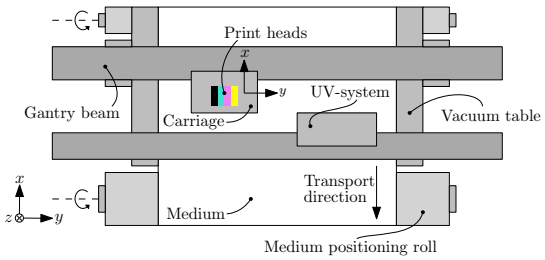

Figure 1.2: *Schematic top view of a wide-format Roll-To-Roll (RTR) printing system.*

A schematic top view of the wide-format RTR printing system is depicted in Figure 1.2. The print heads, dropping the ink on the medium, are located inside the carriage. The carriage moves with a constant speed along the lateral direction of the medium (y-direction). A movement of the carriage from left to right, or vice versa, is called a print-pass. The carriage is attached to the gantry beam, which offers the required motion freedom in longitudinal direction (x-direction). The medium is step-wise transported in between print-passes, with a fixed step size in the x-direction, by rotation of the Medium Positioning Roll (MPR). Medium transportation inevitably leads to positioning errors in the x-direction, which are called MPEs.

1.2 Problem: Medium Positioning Errors

MPEs strongly affect the print quality. These MPEs arise between the medium and the print heads, which are mostly determined by,

1. inaccurate media steps performed by the MPR, e.g., [4]
2. structural errors induced by the media handling, such as friction from the printing surface and hysteresis [11], and
3. errors due to deformation of the medium, caused by changing temperature and humidity [27].

All these components contribute to misalignment of consecutive print-passes, depicted in Figure 1.3.

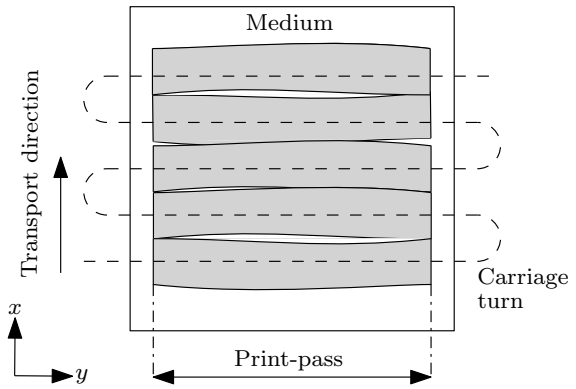

Figure 1.3: *Visualization of Medium Positioning Errors (MPEs) on the medium. The dotted line indicates the carriage trajectory relative to the medium, while the medium is transported in the x-direction.*

Compensation of these MPEs, and thus improving print quality, is currently done by overlapping print-passes [3]. Although overlap means improved print quality, the production speed significantly reduces. Improving positioning accuracy of MPR is nowadays done by using expensive suspensions. Using less expensive suspensions is desired for cost reduction, while maintaining high print qualities.

The challenge is that most contributions to the MPEs are often unknown and dependent on the medium, time, and position. Although these particular described medium-dependent dynamics from [19] can be modeled for a particular medium, the MPEs are different for every medium. Hence, modeling or calibration of these MPEs is time-consuming. Furthermore, accurately positioning the carriage is affected by external disturbances consisting of different frequencies. A Power Spectral Density (PSD) of an MPE measurement is depicted in Figure 1.4 for a particular medium.

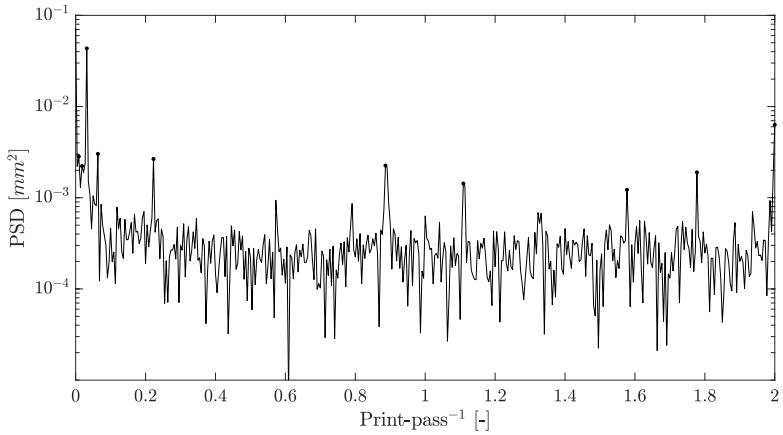

Figure 1.4: *Power Spectral Density (PSD) over the print-passes. The largest peak can be seen at* 0.03182*, which is the frequency of the Medium Positioning Roll (MPR).*

This figure is emphasized in Section 2.1, however a key observation is that multiple components at various frequencies are contributing to the MPEs. Compensation of these periodic components contributing to the MPEs is the main contribution to achieve high printing qualities, i.e., accurate alignment of each print-pass.

1.3 Control Problem

The print accuracy from a control perspective can roughly be divided into three contributions,

1. the ink droplet jetting accuracy [27],
2. the positioning accuracy of the medium, and
3. the positioning accuracy of the print heads.

The ink droplet jetting accuracy (1), is not considered part of this research. Accurate medium positioning beneath the print heads (2), is performed by step-wise transportation of the MPR, depicted in Figure 1.2. However, accurately positioning the medium is a difficult problem due to, e.g., medium-dependent and nonlinear dynamics. Therefore, the aim is to achieve compensation of the MPEs, i.e., accurate alignment of consecutive print-passes, by positioning the print heads in the x-direction (3). This is achieved by movement of the gantry beam in the x-direction, depicted in Figure 1.2.

Compensation of the MPEs is done by using the MPEs as a 'disturbance' for the yet undefined control strategy in the control diagram, depicted in Figure 1.5. The remaining error is the difference between these MPEs and the gantry position in the x-direction. This remaining error is used in this control strategy to compute a compensating reference trajectory to be tracked by the closed-loop system, consisting of the gantry beam and the stabilizing feedback controller.

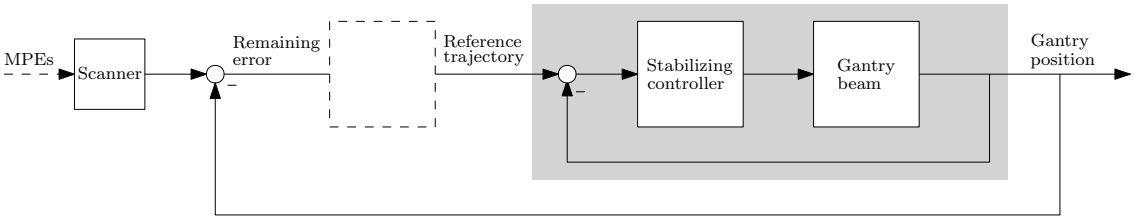

Figure 1.5: *Block diagram of the control problem. The dashed block suggests a potential control strategy. The dashed line indicates a different sample rate, i.e., discrete markers.*

The MPEs are measured through discrete markers on the medium [3], implying a different sample rate, as indicated by the dashed line in Figure 1.5. After one horizontal row of markers is printed, they are measured by an image processing algorithm and upsampled, depicted by the 'scanner' in Figure 1.5. Notice that these marker measurements for each print-pass become available after the print-pass due to scanning and image processing. This implies that the position of the medium with respect to the print heads cannot be measured directly, which makes real-time feedback control unavailable. Furthermore, feedforward control cannot be applied, since disturbances are not known in real-time.

Although the MPE measurements are not available in real-time, their periodicity can be exploited through batch-wise learning control. Learning from previous errors can significantly improve the position performance, due to the repetitive nature of the disturbances. Learning control does not require accurate dynamical models or known signals in real-time, only that the disturbances are repetitive. Most common learning control strategies are Iterative Learning Control (ILC) and Repetitive Control (RC). ILC is used for discontinuous operation, while RC can be used for continuous operations [5]. In [19], ILC is exploited on a wide-format printing system. Although promising results are shown for ILC, RC is more suited for handling continuously repeating disturbances.

In [4], the potential of RC in time-domain is shown, however the theoretical foundations in time-domain often results in large and complex system descriptions, not to mention stability analyses. Hence, it might be more intuitive to address the control problem in frequency-domain RC, which is often preferred by control engineers. In literature, RC in frequency-domain shows promising results, see, e.g., [1, 15, 22, 23].

As depicted in Figure 1.4, multiple components at various frequencies are present in the printing system. Single-period RC, i.e., Standard RC, can only handle one periodic disturbance [4, 10, 15]. Addressing multiple periods with standard RC requires a Least Common Multiple (LCM), hence potential slow learning. Thus, compensation of multiple unrelated periods is investigated by multi-period RC in frequency-domain.

Existing design solutions to compensate for disturbances with multiple periods by multi-period frequency-domain RC is discussed in the next section.

1.4 Existing Design Solutions to Multi-Period Repetitive Control

Potential methods to reject disturbances with multiple unrelated periods by multi-period RC are investigated in [14]. It is suggested to combine multiple repetitive controllers in various structures. Three different structures are given, i.e., the serial structure, the parallel structure and the cascaded structure.

From [14], it follows that the serial structure has difficulties regarding stability and shows insufficient performance if stable at all. The parallel structure, has potential to reject disturbances with multiple unrelated periods. However, stability analysis and design procedures are not well established for this structure. From [6, 16], it follows that independent designs are potentially conservative due to a prior unknown designs in other loops, and shows slow learning as illustrated in this thesis. The cascaded structure has the most favorable properties regarding stability and performance. Yet, design is unclear.

In [26], the cascaded structure is investigated in more detail. It is shown that by combining the repetitive controller in cascaded form, disturbances of multiple periods can be rejected. Although promising results are shown, the design of those repetitive controllers is not straightforward. In [26], it is suggested to design a robust RC design against modeling errors, by using a multiplicative model uncertainty. However, this might result in very conservative designs, since often in practice the modeling error is accurately known, e.g., from Frequency Response Function (FRF) measurements.

These observations give rise to designing the repetitive controllers in a sequential manner, where modeling errors are explicitly accounted for in sequential designs. Sequential design is commonly done in practice for feedback control [13, 17, 21], yet its potential for RC is unexplored.

1.5 Contributions

The latter results in the following research question:

How to sequentially design multiple repetitive controllers to achieve rejection of periodically recurring medium positioning errors in wide-format roll-to-roll printing systems?

This research question is divided into the following research contributions:

1. Characterization of repetitive medium positioning errors in wide-format roll-to-roll printing systems.
2. Development of a sequential design approach for multi-period RC.
   (a) Investigation of various control configurations for multiple repetitive controllers.
   (b) Development of a sequential design procedure.
3. Validation of the developed sequential design approach by means of simulation, using a parametric model of the gantry-beam in the x-direction.
4. Experimental validation of the developed sequential design approach for multi-period RC on a wide-format roll-to-roll printing system.

1.6 Outline

This thesis is organized as follows. Chapter 2 describes the industrial wide-format RTR printing system and the MPEs in more detail. Next, a single-period RC framework, i.e., standard RC, is discussed in Chapter 3, including a detailed background analysis, stability analysis, and design procedure. This knowledge is extended towards sequential design for multi-period RC discussed in Chapter 4. Two different control structures are presented, followed by stability analysis. The developed sequential design procedure is presented and validated with simulations. In Chapter 5, the developed theory is validated on a wide-format RTR printing system. Finally, a conclusion is drawn and recommendations for future work are presented in Chapter 6.

Chapter 2

Experimental Setup

In this chapter, the experimental setup is described in more detail, and the MPEs are analyzed. In Chapter 5, the developed sequential design framework for multi-period RC is applied to the setup presented here. The setup is an industrial wide-format RTR printing system from Océ Technologies.

The outline of this chapter is as follows. First, characterization of the repetitive MPEs is given, showing that the MPEs are caused by multiple fundamental frequencies. Second, a detailed system description is presented, to define the control objective and control variable. Finally, the plant and controller dynamics are shown.

2.1 Characterization of Repetitive Medium Positioning Errors

In this section, the repetitive MPEs to be tracked by the gantry beam are investigated. A contribution to MPEs, as mentioned in Section 1.2, are inaccurate media steps performed by the MPR. The resulting MPEs, typically occurring in wide-format RTR printing systems, can roughly be divided into three components, see, e.g., [19].

1. **Translational**: The radius of the MPR may deviate from the average over its circumference, i.e., ellipsoidal shape. This results in a translational position error with respect to the print heads, where the medium is either translated too far or too little.
2. **Rotational**: The axle of the MPR is not exactly parallel with respect to the center-line of the suspension. This is called a wobble effect and results in a rotational position error with respect to the print heads.
3. **Parabolic**: The suspension is bending due the weight of the MPR. This results in a parabolic position error with respect to the print heads. Bending of the media roll contributes to this parabolic position error as well. This position error is slowly changing according to the diameter of the media roll [3].

The MPEs show periodic behavior over consecutive print-passes. The period length depends on the circumference of the MPR and demanded steps size. An example measurement is depicted in Figure 2.1 on the left hand-side, with period length 31 print-passes. The corresponding PSD is depicted on the right hand-side. In this particular measurement, each discrete marker is printed with a four-pass mode, i.e., four print-passes to complete the discrete marker.

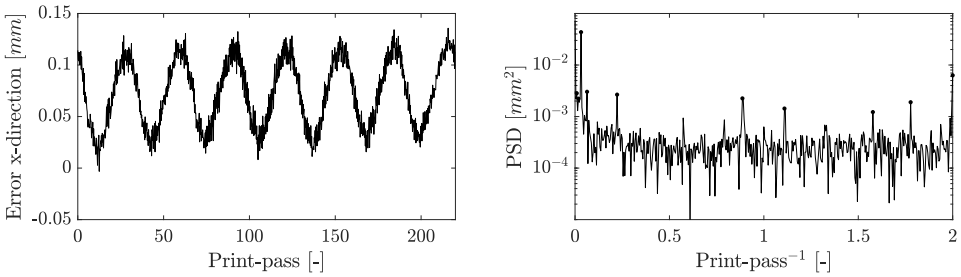

Figure 2.1: *Error in the x-direction as a function of print-passes, measured at the right hand-side of the medium, see 2.2, and its corresponding Power Spectral Density (PSD).*

The example measurement given in Figure 2.1 corresponds with the discrete markers on the right hand-side of the medium, as marked in Figure 2.2 by the yellow oval shape. From each marker in this yellow oval shape, an error in the x-direction is measured, which is shown in Figure 2.1 as function of the print-passes. Notice that 220 markers are printed in this example, i.e., 7 full rotation of the MPR. Similar plots are obtained from the other printed markers, e.g., shifting the yellow oval shape to the left set of markers.

From the PSD in Figure 2.1, it can already be observed that multiple frequencies are present in the system. The largest peak corresponds with the frequency of the MPR, i.e., 0.03182 (≈ 31 print-passes). Although Figure 2.1 is given in print-passes, the corresponding frequencies can be reconstructed to a time-domain signal, as illustrated in Figure 2.3. Next, the printed marker measurements are illustrated for a wide-format RTR printing system in Figure 2.2.

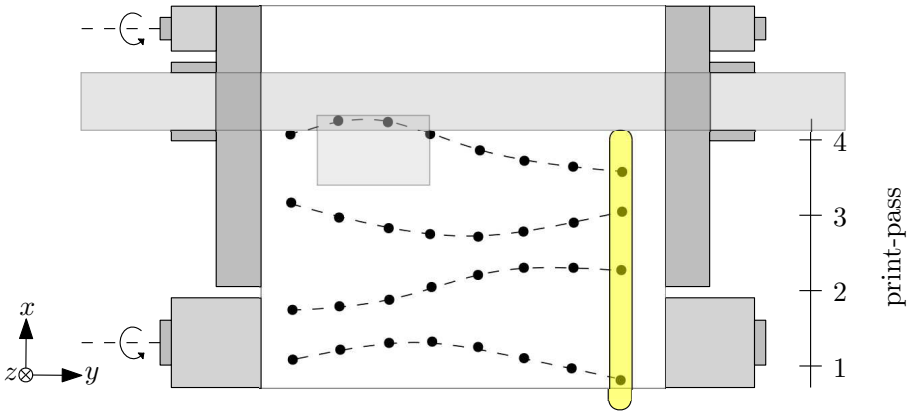

Figure 2.2: *Illustration of the discrete markers for four print-passes on a wide-format Roll-To-Roll (RTR) printing system. Each • represent a printed marker, and the dotted line is a reconstruction of the markers during a print-pass. The yellow oval shape on the right hand-side corresponds with the measurement depicted in Figure 2.1.*

Each printed marker measurement, depicted in Figure 2.2, can be divided in the following sequence of steps.

1. The markers are printed on the medium. Assume that one horizontal row of markers (•) are printed in one print-pass from right to left in Figure 2.2.

2. The image processing algorithm on the carriage scans one horizontal row of markers for each print-pass from left to right.

3. Next, a smooth curve is fitted through the marker measurement, depicted by the dotted line in Figure 2.2. This represents a time-domain reconstruction of an MPE, depicted in Figure 2.3.

4. The MPR performs a step-wise transportation of the medium, and the sequence is repeated.

In Figure 2.3 the reconstruction of the MPEs in x-direction of Figure 2.2 is shown for each horizontal line of printed markers, i.e., each scan from left to right. The grey areas indicate where the actual printing takes place, i.e., where the discrete markers are printed. The white areas in between indicates where the carriage accelerates and decelerates to change direction, i.e., 'turns', as depicted in Figure 2.4. This is also where a fourth-order step signal is computed to connect each scan of the discrete markers.

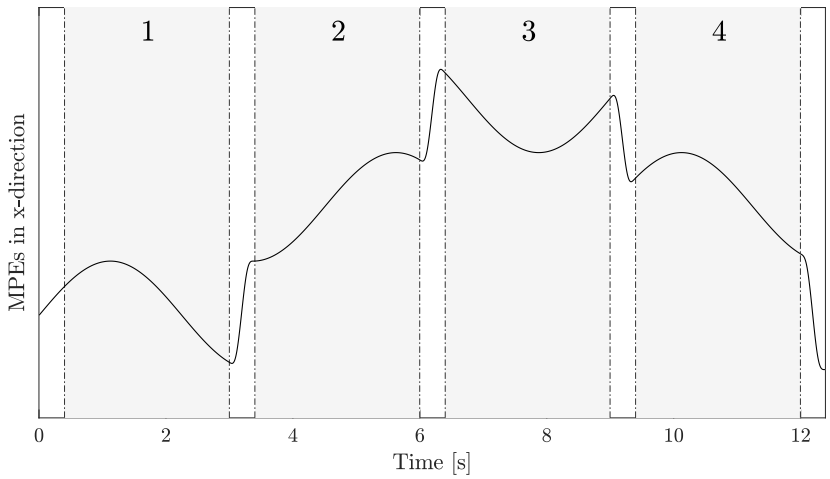

Figure 2.3: *Time-domain signal reconstructed from the discrete marker measurements in the x-direction. The grey areas indicate where the printing takes place and the white areas represent a step of the gantry beam, to connect each reconstruction of the marker measurements.*

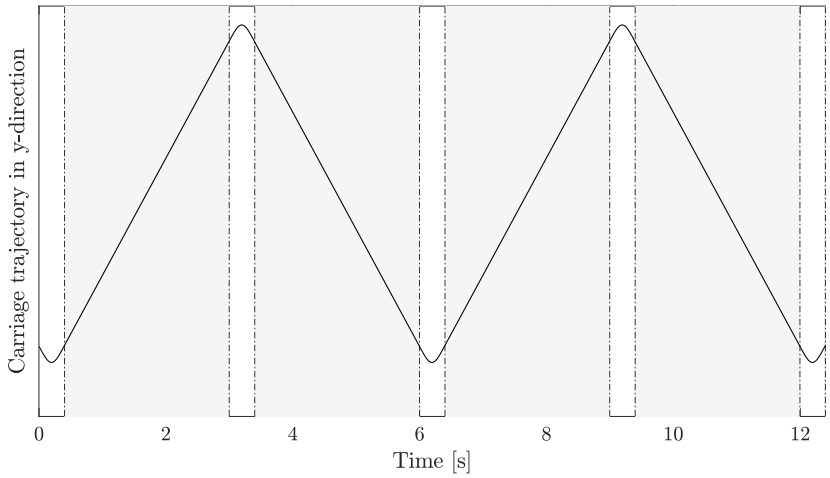

Figure 2.4: *Reference trajectory of the carriage in y-direction. The grey areas indicate where the printing takes place* ≈ 2.6 *[s] and the white areas in between indicate the turning time of the carriage* ≈ 0.4 *[s].*

In Figure 2.4 the reference trajectory of the carriage is illustrated. The carriage has a turning time of 0.4 $[s]$ and the print-pass length is (approximately) 3 $[s]$. During the print-passes, the MPEs, depicted in Figure 2.3, should be tracked by the gantry beam in the x-direction. The next section describes the system in more detail.

2.2 System Description

A schematic side-view of the considered wide-format RTR printing system is given in Figure 2.5. The printing system can be seen as two subsystems.

1. The gantry beam with carriage moving in the x-direction. The input of the gantry beam are voltages to the DC motors, located on the left and right side of the gantry beam, and the outputs are encoders on each side of the gantry beam, depicted in Figure 2.5.

2. The MPR transporting the medium beneath the print heads. The input is voltage to the DC motor driving the MPR, and the output is measured with a rotary encoder, depicted in Figure 2.5.

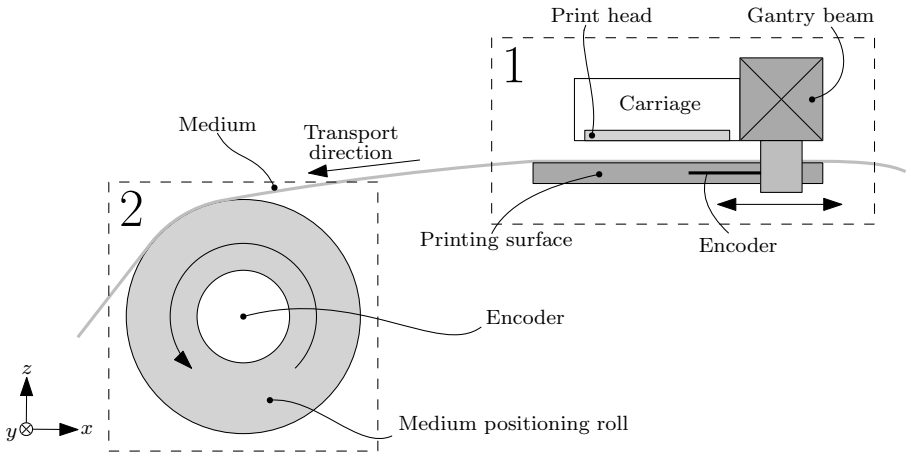

Figure 2.5: *Schematic side-view of the wide-format Roll-To-Roll (RTR) printing system.*

As mentioned in Section 1.1, the MPR performs a step-wise transportation of the medium beneath the print heads by rotating counterclockwise. This transportation of the medium results in MPEs with respect to the print heads due to many causes, given in Section 1.2. The gantry beam should compensate for these errors in the x-direction. Therefore, the reconstructed MPEs are used as a disturbance v to be tracked by the gantry beam in the following control scheme, depicted in Figure 2.6. Where G denotes the dynamics of the gantry beam in the x-direction, K denotes a stabilizing controller, and R an RC framework.

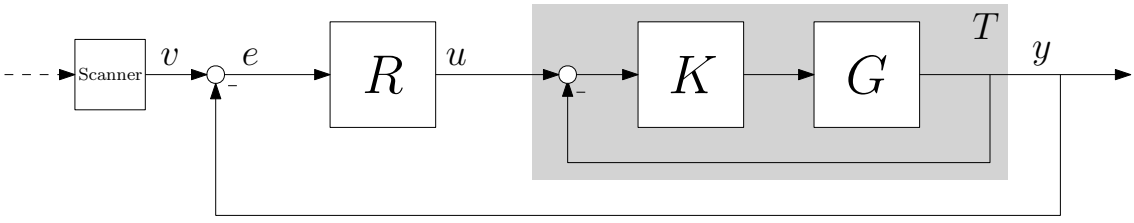

Figure 2.6: *Control scheme of the gantry beam, where the aim is to minimize the error e. The scanner, scans and reconstructs a time-domain signal on the sample frequency of the system.*

The aim of this control scheme is to minimize the error e beneath the print heads in the x-direction. The error in the y-direction is solved by timing the ink jetting droplets and is not within the scope of this thesis. Therefore, the control variable is the position of the print heads in the x-direction, i.e., denoted by y. Hence, compensation of the MPEs is achieved by computing a compensating reference trajectory u with the RC framework. This is periodically updated by the RC framework and consequently tracked by the gantry beam. Potential RC frameworks are discussed in the forthcoming chapters.

2.3 System Dynamics

The system dynamics and corresponding plant models are given in this section. The system dynamics of the gantry beam in the x-direction, i.e., G, is identified by a frequency response measurement. White noise is used as input F_x for the motors and the encoders on each side of the gantry beam are used as outputs, i.e., collocated. From these two outputs, a transformation is applied to obtain the motion in the x-direction, see, e.g., [4, 19]. This results in the FRF measurement from F_x to x, depicted in Figure 2.7 by G.

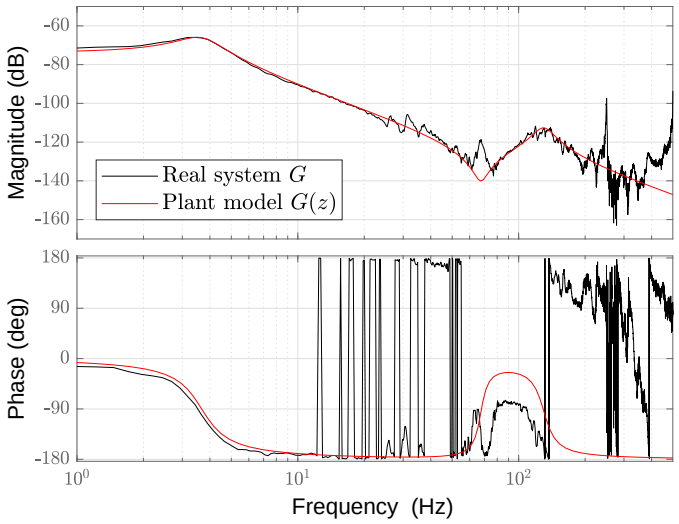

Figure 2.7: *Bode diagram of the plant G and plant model $G(z)$.*

The discrete-time plant model $G(z)$ is obtained by fitting two modes of the system, i.e., 3.7 Hz and 130 Hz, and is discretized by using Zero-Order Hold (ZOH), resulting in a fourth-order transfer function given by,

$$G(z) = \frac{1.92 \cdot 10^{-7} z^3 - 1.57 \cdot 10^{-7} z^2 - 1.45 \cdot 10^{-7} z + 1.75 \cdot 10^{-7}}{z^4 - 3.26 z^3 + 4.37 z^2 - 2.96 z + 0.85}. \tag{2.1}$$

Remark 2.1. Notice that the FRF measurement, depicted in Figure 2.7, shows a resonance frequency at 70 Hz. This is obtained due to environmental circumstances, however not of importance for modeling.

The stabilizing feedback controller $K(z)$ consists of an integrator, lead-lag filter and a second order low-pass filter. Discretizing by using ZOH results in a fourth-order feedback controller given by,

$$K(z) = \frac{1.86 \cdot 10^4 z^4 + 1.52 \cdot 10^3 z^3 - 3.87 \cdot 10^4 z^2 + 9.8 \cdot 10^2 z + 1.76 \cdot 10^4}{z^4 - 3.11 z^3 + 3.78 z^2 - 2.14 z + 0.47}. \tag{2.2}$$

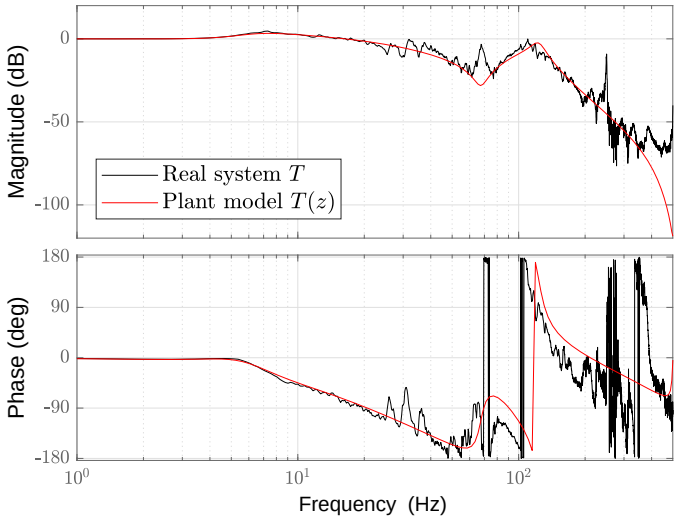

Figure 2.8: *Bode diagram of the plant T and plant model $T(z)$.*

The stabilizing controller $K(z)$ is implemented to obtain the complementary sensitivity function $T = GK(1 + GK)^{-1}$, depicted in Figure 2.8. The plant model $T(z)$ is non-minimum phase and achieves a closed-loop bandwidth of 24 Hz.

To conclude this chapter, the repetitive nature of the MPEs is exploited and the experimental setup is given in detail. In the next chapter, the theory and design for standard RC are discussed, which forms the basis to reject these repetitive MPEs.

Chapter 3

Single-Period Repetitive Control

RC can achieve perfect disturbance rejection or reference tracking of an exogenous repetitive signal. This is realized by the Internal Model Principle (IMP), which states that perfect asymptotic rejection or tracking is achieved if an internal model of the input signal generator is included in the feedback loop.

In this chapter, the theory and design of standard RC is discussed in detail. The goal is to develop a strong basis for multiple repetitive controllers and the corresponding structures, which are discussed in the forthcoming chapters. The elaborations are done in frequency-domain, which is typically presented in literature as well [1, 12, 15]. Furthermore, the repetitive controller is connected by a feedback loop, since the repetitive controller computes a reference trajectory for the closed-loop system, as discussed in Section 1.3.

First, the control setup is discussed where the fundamentals of RC are given. Additionally, the background on the IMP is discussed, with applications on a standard feedback loop and RC. Furthermore, stability of RC is explained in detail, which results in generic stability and design conditions. Finally, a design procedure is given, where the learning filter, robustness filters, and learning gain are discussed.

3.1 Repetitive Control Setup

The practical control problem states that MPEs, mostly introduced by the MPR, should be followed by the print heads in the x-direction. These MPEs are considered as a disturbance in the control problem. Hence, focusing on RC design for a general disturbance v on a closed-loop system, results in the control configuration depicted in Figure 3.1, where the repetitive controller R is connected in an extra feedback loop.

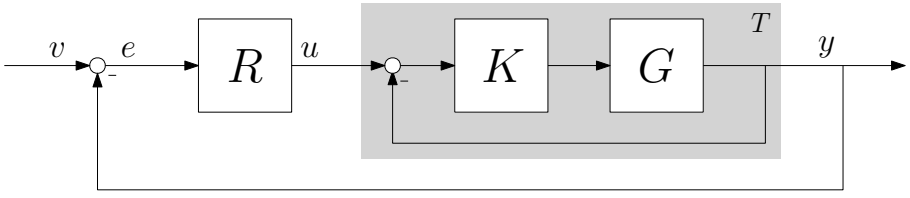

Figure 3.1: *Control configuration with repetitive controller in a feedback loop on the closed-loop system T.*

The control configuration, depicted in Figure 3.1, consists of a discrete-time Linear Time-Invariant (LTI) Single-Input Single-Output (SISO) system with $G \in \mathcal{R}(z)$ the plant, $K \in \mathcal{R}(z)$ the stabilizing feedback controller, and $R \in \mathcal{R}(z)$ as the repetitive controller. The system $T \in \mathcal{RH}_\infty(z)$ is denoted by the complementary sensitivity function, i.e., $T = GK(1 + GK)^{-1}$. The aim is to minimize the tracking error e, by updating input signal u, where after the output y of G follows the disturbance v. The disturbance v is a periodic exogenous disturbance with period length $N \in \mathbb{N}$, e.g., $v(k) \in \mathbb{R}$ with $v(k+N) = v(k)$. Where k

denotes the discrete time variable and N the number of samples delay. Furthermore, the error propagation $e = v - y$ is given by,

$$e = (1 + TR)^{-1}v = S_R v, \tag{3.1}$$

with $S_R \in \mathcal{R}(z)$ as the modifying sensitivity function.

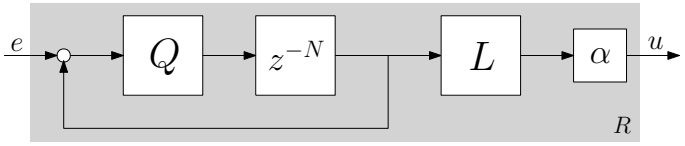

Figure 3.2: *Repetitive controller scheme.*

The repetitive controller R, depicted in Figure 3.2, is given by,

$$R = (1 - z^{-N}Q)^{-1}\alpha L z^{-N} Q. \tag{3.2}$$

This repetitive controller consists of a memory loop, robustness filter $Q \in \mathcal{RL}_\infty(z)$, learning filter $L \in \mathcal{RL}_\infty(z)$, and learning gain $\alpha \in \mathbb{R}$. Note that R should be causal, and Q and L are allowed to have finite preview. The necessary implementations of the filters and gains are discussed in forthcoming sections.

Remark 3.1 (RC configuration with RC as add-on type [10, 15])**.** Typically in literature the control configuration is given as in Figure 3.3. Here, the repetitive controller is connected by an add-on type controller. However, from design perspective there is no difference in the control configuration (3.1) or (3.3).

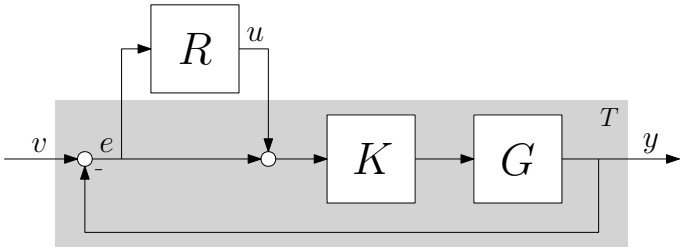

Figure 3.3: *Control configuration with repetitive controller as add-on controller.*

The tracking error of Figure 3.3 is given by,

$$e = (1 + GK(1 + R))^{-1}v = S_R S v, \tag{3.3}$$

with $S = (1+GK)^{-1}$ as the sensitivity function. Stability and design conditions are in both control configurations related to the modifying sensitivity function S_R, assuming that $S \in \mathcal{RH}_\infty(z)$. Since the repetitive controller should compute a reference trajectory for the closed-loop system, the control configuration in Figure 3.1 is considered in this research.

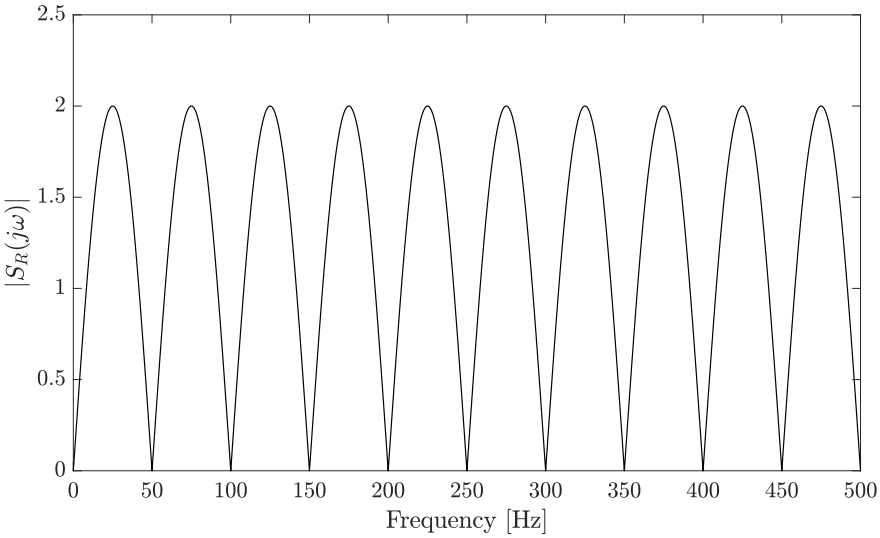

Figure 3.4: *Magnitude of the modifying sensitivity function, with period length $N = 20$ samples. The learning filter is chosen as $L = T^{-1}$, the robustness filter as $Q = 1$, and learning gain as $\alpha = 1$.*

To conclude, an example of the modifying sensitivity function S_R is depicted in Figure 3.4, where the disturbance frequency is chosen as 50 Hz, i.e., the period length is $N = 20$ samples with sample frequency 1000 Hz. Here, it is clearly visible how the repetitive controller suppresses the considered disturbance frequency and all its higher harmonics up to the Nyquist frequency. Note that disturbance rejection or reference tracking is achieved at the expense of amplification of intermediate frequencies, due to Bode's sensitivity integral [23]. The fact that in Figure 3.4 the disturbance frequency and all higher harmonics are suppressed is related to the IMP, which is explained in the next section.

3.2 Background: Internal Model Principle

In this section, the IMP is discussed, which is a fundamental concept for RC. This principle assures that RC is capable of achieving perfect disturbance rejection or reference tracking of an exogenous repetitive signal. First, the theoretical part of the IMP is discussed. Thereafter, the application on standard feedback control and RC is given to show that this concept is very general. Finally, a simple example is given to illustrate the effectiveness of the IMP, and thus RC.

Consider the closed-loop control configuration of a discrete-time LTI SISO system, depicted in Figure 3.5.

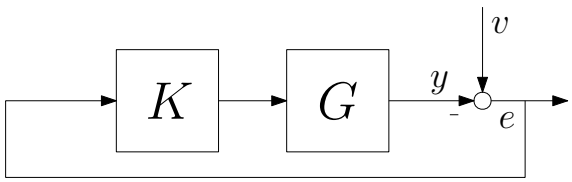

Figure 3.5: *Control configuration of a closed-loop system.*

The error propagation $e = v - y$ is defined as,

$$e = (I + GK)^{-1}v = Sv, \tag{3.4}$$

with $S \in \mathcal{RH}_\infty$ the sensitivity function from the disturbance v to the error e. The control objective of

Figure 3.5 is to achieve perfect asymptotic disturbance rejection, i.e.,

$$\lim_{t\to\infty}(v(t)-y(t))=0. \tag{3.5}$$

Let the z-transformation of the discrete-time disturbance $v(t)$ be given by,

$$V(z)=\frac{N_v(z)}{D_{v,s}(z)D_{v,u}(z)}. \tag{3.6}$$

Where $N_v(z)$ is known, $D_{v,s}(z)$ is the polynomial with the stable poles, i.e., poles in $\mathbb{D}$, and $D_{v,u}(z)$ the polynomial with the unstable poles, i.e., poles in $\mathbb{E}\cup\mathbb{T}$. Assuming that $V(z)$ is proper, results in the following theorem.

Theorem 3.1 (Internal Model Principle [8, 12])**.** *If the disturbance $v(t)$ has $D_{v,u}(z)$ as the internal model, then using a controller of the form,*

$$K(z)=\frac{1}{D_{v,u}(z)}\frac{N_k(z)}{D_k(z)}, \tag{3.7}$$

in the standard one degree-of-freedom control configuration can asymptotically reject the effect of the disturbance, if

1. *the closed-loop system is asymptotically stable, and*
2. *no pole-zero cancellation of the internal model $D_{v,u}(z)$ and $G(z)$ are present.*

Thus, the marginally stable poles of the repetitive disturbance signal, should be included in the denominator of the controller $K(z)$, such that these poles are canceled by the closed-loop transmission zeros in the sensitivity transfer function [8].

Proof. Let the plant model $G(z)$ be given by,

$$G(z)=\frac{N_g(z)}{D_g(z)}. \tag{3.8}$$

Assume that no pole of the generating polynomial $D_{v,u}(z)$ is a zero of the plant $G(z)$. Otherwise, pole-zero cancellations would occur, causing internal instability. Let the z-transformation of the sensitivity function (3.4) be given by,

$$S(z)=(I+G(z)K(z))^{-1}=\frac{D_{v,u}(z)N_k(z)N_g(z)}{D_{v,u}(z)D_k(z)D_g(z)+N_k(z)N_g(z)}. \tag{3.9}$$

Now, rewriting the error propagation in z-domain results in,

$$E(z)=S(z)V(z)=S(z)\frac{N_v(z)}{D_{v,s}(z)D_{v,u}(z)}=\frac{N_k(z)N_g(z)N_v(z)}{A_{cl}(z)}\frac{D_{v,u}(z)}{D_{v,s}(z)D_{v,u}(z)}. \tag{3.10}$$

In (3.10) can be seen that the unstable part of $V(z)$, i.e., $D_{v,u}(z)$, is canceled in the denominator of (3.10) by including this part in the denominator of $K(z)$. Now, all poles of $V(z)$ in $\mathbb{E}\cup\mathbb{T}$ are canceled, which yields the inverse z-transformation of $E(z)$ as,

$$\lim_{t\to\infty}e(t)=0, \tag{3.11}$$

assuming that denominator of (3.9), i.e., $A_{cl}(z)=D_{v,u}(z)D_k(z)D_g(z)+N_k(z)N_g(z)$, has stable roots. □

3.2.1 Application to Feedback Control: Constant Signals

If the system is subjected to a constant disturbance signal, then the internal model is an integrator, depicted in Figure 3.6.

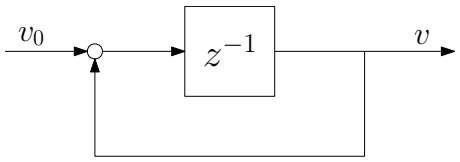

Figure 3.6: *Integrator.*

A constant disturbance signal can be seen as a repetitive signal with period length $N = 1$ sample. If the sequence $v_0(k) = v(0)$ is fed in Figure 3.6 then $v(k)$ appears at the output. This z-transformation is then given by,

$$V(z) = \frac{z^{-1}}{1 - z^{-1}} V_0(z) = M_i(z) V_0(z), \tag{3.12}$$

with the fractional clearly being an integrator. According to Theorem 3.1, the internal model of $M_i(z)$, i.e., the unstable part of the denominator of $M_i(z)$, should be in the feedback controller $K(z)$. This is the reason that no steady state error occurs, in case of a step signal in an LTI feedback control system, if an integrator is in the feedback controller [12].

3.2.2 Application to Repetitive Control: N-Periodic Signals

In case of N-periodic signals, the internal model is a Periodic Signal Generator (PSG), depicted in Figure 3.7. This PSG is basically a memory block and a positive feedback loop. The size of N is determined by the disturbance frequency f_d and the sample frequency f_s, i.e., $N = \frac{f_s}{f_d}$. Perfect rejection is possible if f_d is known and fixed.

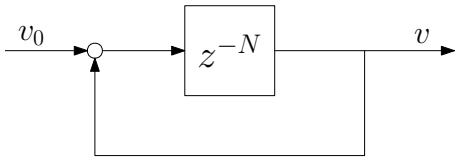

Figure 3.7: *Periodic Signal Generator (PSG).*

Feeding the following periodic sequence $v_0(k) = v_0(0), ..., v_0(N-1)$ in the memory loop of Figure 3.7, results in a periodic signal $v(k)$ at the output. The z-transformation is then given by,

$$V(z) = \frac{z^{-N}}{1 - z^{-N}} V_0(z) = M_r(z) V_0(z), \tag{3.13}$$

with $M_r(z)$ having N poles uniformly distributed on the unit circle.

According to Theorem 3.1, the unstable part of the denominator polynomial of $M_r(z)$ should be included in the feedback controller $K(z)$ in Figure 3.5, to achieve asymptotically disturbance rejection. Not only is asymptotically disturbance rejection achieved for an exogenous repetitive signal with frequency f_d, but also for all higher harmonics up to the Nyquist frequency $\frac{f_s}{2}$. This can be seen by using $z = e^{j\omega T_s}$ in (3.13), with $\omega = 2\pi f$ and $T_s = \frac{1}{f_s}$, i.e., the sample time. The denominator of (3.13) is zero for the frequencies f being equal to f_d and all higher harmonics, i.e., $f = pf_d$, with $p \in \mathbb{Z}$. This means infinite gain for the disturbance frequency f_d and for all higher harmonics. Note that infinite gain is also achieved for $f = 0$.

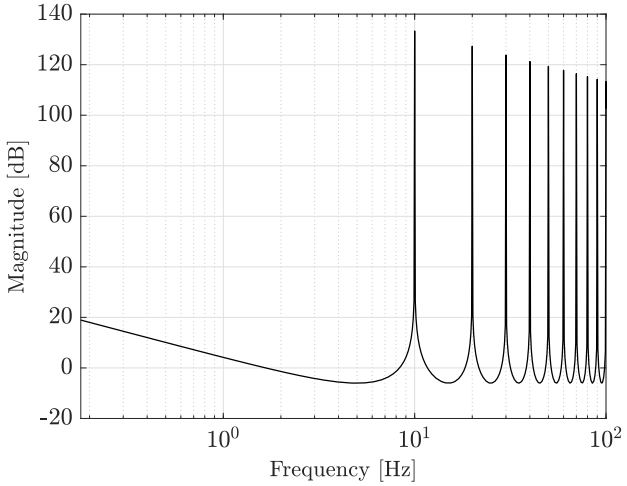

Figure 3.8: *Bode magnitude diagram of the memory loop with $f_d = 10$ Hz, and $f_s = 1000$ Hz.*

In Figure 3.8 an example is depicted of a memory loop, with $f_s = 1000$ Hz, and $f_d = 10$ Hz. From this figure, it is clear that high gain disturbance rejection or reference tracking for each signal with 10 Hz and all higher harmonics is achieved. Furthermore, consider the following example, where the simplicity and effectiveness of RC is visualized in time-domain.

Example 3.1. The control configuration in Figure 3.1 with the repetitive controller R as in Figure 3.2 are used in this example. The disturbance frequency is chosen as 1 Hz, i.e., period length $N = 1f_s$ samples, with $f_s = 1000$ Hz. For simplicity let $T = L^{-1} = 1$, and no robustness filter, i.e., $Q = 1$. The learning gain α equals 0.5 to illustrate the learning process.

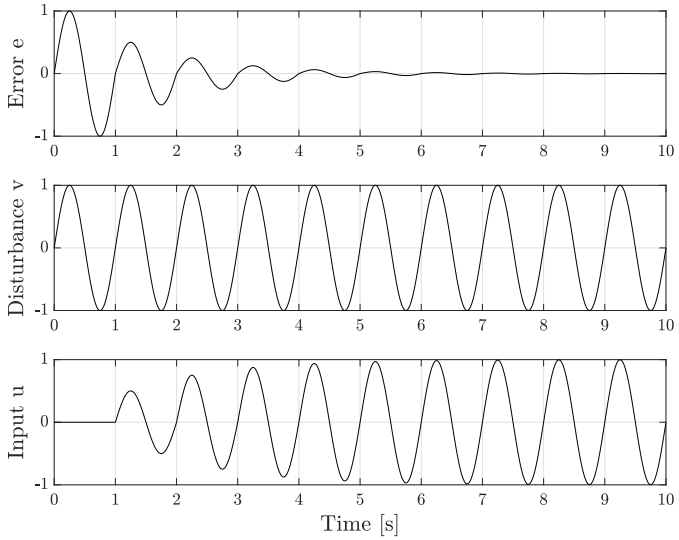

Figure 3.9: *Resulting signals of simple example.*

The disturbance signal v is depicted in Figure 3.9 (middle), together with the error signal e (top) and the input signal u (bottom), i.e., the output of the repetitive controller. Notice how the signal in the memory loop, i.e., u, starts to look like the disturbance, and consequently, the error signal is suppressed in the process.

The learning filter L and learning gain α, depicted in Figure 3.2, are not part of the internal model. This means that they do not influence the IMP. The robustness filter Q on the other hand does. It is part of the memory loop, as depicted in Figure 3.2, which indicates that if $Q \neq 1$, the IMP is violated. This is true after the cut-off frequency, which indicates that the repetitive controller is not capable of perfect disturbance rejection or reference tracking after and around the cut-off frequency.

Despite that, overall stability of the closed-loop system with the repetitive controller should be guaranteed. From the internal model (3.13), it can already be observed that N unstable open-loop poles are added to the closed-loop system, depending on the robustness filter Q. Hence, stability analysis is covered in the next section.

3.3 Stability Analysis

To guarantee stability of the closed-loop system depicted in Figure 3.1, first the feedback controller K should stabilize the plant G. Second, the repetitive controller should not destabilize the system. Hence, stability of Figure 3.1 is guaranteed if all poles of S_R are on the open unit disc. However, checking all the pole locations of S_R is inconvenient, especially if no (accurate) parametric model is available. Furthermore, N can grow very large, which might introduces many poles on the unit circle, depending on the robustness filter.

Factorization

The solution to avoid checking on all possible poles on the unit circle can be found by factorization of S_R. Using (3.2) in the modifying sensitivity function yields the following derivation,

$$\begin{aligned} S_R &= (1 + T(1 - z^{-N}Q)^{-1}\alpha L z^{-N}Q)^{-1}, \qquad (3.14)\\ &= \big((1 - z^{-N}Q + \alpha TL z^{-N}Q)(1 - z^{-N}Q)^{-1}\big)^{-1},\\ &= (1 - z^{-N}Q)(1 - (1 - \alpha TL)z^{-N}Q)^{-1}. \qquad (3.15) \end{aligned}$$

This factorization is visually displayed as an equivalent error system, depicted in Figure 3.10. The first factor of (3.15) only shifts the disturbance by N samples and subtracts this from the original disturbance, which goes to zero if N equals the repetitive period of v.

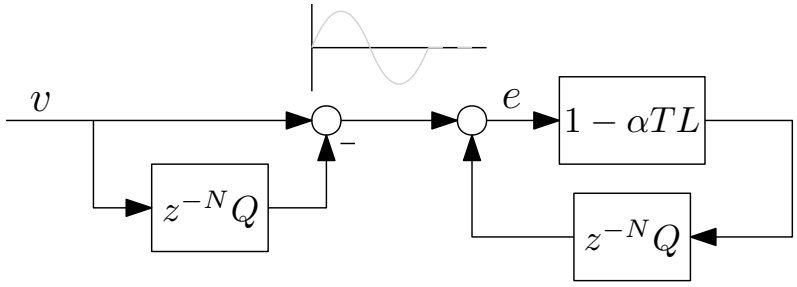

Figure 3.10: *Equivalent error system.*

Stability theorem

Now, the Nyquist stability criterion can be applied on the second term of (3.15) [21]. With $(1 - H(z))$ as the return difference and $H(z) = (1 - \alpha TL)z^{-N}Q$ as the loop-gain, results in the following Nyquist stability theorem for RC.

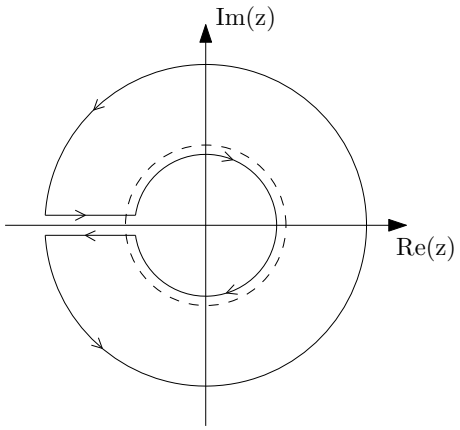

Figure 3.11: *The Nyquist contour* Γ *consists of an inner circle with radius* 1 *and an outer circle with radius* ∞*. This contour is closed by two parallel lines form* -1 *to* $-\infty$ *and vice versa, infinitely close to the real axis. The smaller dotted circle is the unit circle* $\mathbb{T}$ *with radius* 1*.*

Theorem 3.2 (Nyquist stability theorem for SISO RC)**.** *Consider the control configuration of Figure 3.1, with R as in* (3.2)*, suppose all poles of* T*,* L*, and* Q *are on the open unit disc, and assume no unstable pole-zero cancellations between* $(1 - z^{-N}Q)$ *and* $(1 - H(z))$ *in* (3.15)*. Then the closed-loop system* (3.1) *is stable if and only if the image of* $(1 - \alpha TL)z^{-N}Q$

1. *makes no encirclement of the point* $1 + 0j$*, and*
2. *does not pass through the point* $1 + 0j$*,*

as z *goes around the Nyquist contour* Γ *in Figure 3.11.*

Remark 3.2. The importance of the factorization in (3.15) can be seen in Theorem 3.2. No open-loop unstable poles are present in the loop-gain $H(z)$. Which indicates that no encirclements of the point $1 + 0j$ for z going around the Nyquist contour Γ are required for stability, making Theorem 3.2 a practical stability condition. Alternatively, applying the Nyquist stability criterion directly on $S_R = (1 + TR)^{-1}$, with $Q = 1$ in (3.2) for the moment, yields N open-loop unstable poles on the unit circle for the loop-gain TR. Consequently, the image of $(1 + TR)$ should have N times counterclockwise encirclements of the origin for z going around the Nyquist contour Γ. Hence, yielding no closed-loop poles outside the open unit disc, i.e., $Z = 0$. In this case, the contour Γ should even be adapted. Now, semicircular indentations into the unit circle should be made around the poles on the unit circle [7]. Hence, less practical.

Although Theorem 3.2 provides a necessary and sufficient stability condition, it does not guarantee stability if the repetitive controller is implemented with different period length N. This, together with the fact that Theorem 3.2 is still inconvenient for design, motivates the following lemma.

Lemma 3.3. *Under the assumptions of Theorem 3.2 and* $H(z)$ *is strictly proper, the closed-loop system* (3.1) *with* R *as in* (3.2) *is stable for all* $N \in \mathbb{N}$ *if*

$$|(1 - \alpha T(e^{j\omega})L(e^{j\omega})))Q(e^{j\omega})| < 1 \quad \forall \omega \in [0, \pi]. \tag{3.16}$$

Proof. First, if $H(z)$ is strictly proper, which is typically the case for sufficiently large N, only the contour around unit circle needs to be evaluated in Theorem 3.2. Since evaluation of the outer circle at ∞ of the Nyquist contour Γ, results in $\lim_{|z|\to\infty} H(z) = 0$, i.e., it never results in an encirclement of the point $1 + 0j$. Furthermore, the parallel lines along the real axis of the Nyquist contour Γ, only results in behavior of $H(z)$ inside the unit circle along the real axis. Finally, note that $|z^{-N}| = 1$ for z on the unit circle, hence (3.16) implies stability for all $N \in \mathbb{N}$. Consequently, using the small gain theorem [21], results in (3.16). □

Lemma 3.3 has a high level of practical usability, since it enables RC design independent of N. Although it is not necessary for stability, it makes visual verification of stability very useful and design more practical.

3.4 Design Procedure

The learning filter, robustness filter, and learning gain each have different properties. In the following sections is described how to design these filters and gain. First, a two-step design procedure is given for single-period RC [10, 25].

Procedure 3.1 Frequency-domain single-period RC design

1. Given a parametric model of T, design $L(z)$ as an approximate stable inverse, i.e., $L(z) = \alpha T(z)^{-1}$, with learning gain $0 < \alpha < 2$.
2. Given a FRF of T, design $Q(z)$ such that (3.16) holds.

3.4.1 Learning Filter

The learning filter is added to the memory loop to compensate for closed-loop behavior of Figure 3.1. According to (3.16), ideally the learning filter should be the approximate inverse of the complementary sensitivity function, i.e., $L = T^{-1}$. This inversion is mostly approximated by a parametric model of T. However, if $T(z)$ is non-minimum phase, the resulting learning filter will have unstable poles. For this reason, $L(z)$ can be designed using the Zero Phase Error Tracking Controller (ZPETC) algorithm [25], or alternative algorithms such as, Finite Impulse Response (FIR) models [24] and $\mathcal{H}_\infty$-synthesis with preview [2]. The learning filter is allowed to be non-causal, i.e., having finite preview, which is crucial in compensation for the non-minimum phase zeros of $T(z)$. Non-causality can be compensated in the implementation, depicted in Figure 3.12. Now the causal filter is given by $L_c = z^{-n_L} L$ [1].

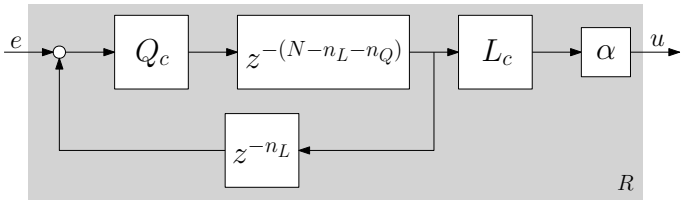

Figure 3.12: *Repetitive controller scheme with non-causal filters.*

3.4.2 Robustness Filter

The learning filter is based on the inverse of a parametric model of T. However, any mismatch between the parametric model $T(z)$ and real system T, might cause stability issues, especially at higher frequencies. Therefore, the robustness filter $Q(z)$ is introduced, which is designed as a low-pass filter with the cut-off frequency dependent on the modeling error. As depicted in Figure 3.2, the robustness filter should not influence the phase of the signal. This is why the filter is usually chosen as a zero-phase low-pass filter [15], e.g., a non-causal zero-phase low-pass FIR filter. Any preview of the robustness filter can be compensated in the implementation as depicted in Figure 3.12, with the causal filter as $Q_c = z^{-n_Q} Q$ [1].

3.4.3 Learning Gain

Finally, the learning gain α is a trade-off between noise amplification, speed of convergence and robustness against changing period lengths N [23]. A small α gives less intermediate disturbance amplification, since it results in narrower notches of S_R, however the controller becomes more sensitive to changing period lengths. A larger α results in the opposite. According to 3.16, the learning gain should be chosen between $0 < \alpha < 2$. Lower or higher than 1 results in slower convergence. Even though stability is verified with these boundaries, $\alpha \in (1, 2)$ is not recommendable. It only becomes less sensitive to change in period

length, which is typically known in many systems. Moreover, it results in slower convergence and gives more disturbance amplification of intermediate frequencies.

Remark 3.3. In this work it is assumed that the period length N is exactly known, however the controller structure can be extended using multiple memory loops to deal with uncertain N, e.g., [22, 23].

To conclude this chapter, the theoretical foundations for RC are given. Those foundations are used in the next chapter to develop a multi-period RC framework.

Chapter 4

Multi-Period Repetitive Control: Sequential Design

Multiple repetitive controllers are capable of perfect disturbance rejection or reference tracking of repetitive signals with multiple periods. In many systems the disturbance consists of more than one fundamental frequency, which is typically known a prior. In case of the printing system, as described in Chapter 2, multiple frequencies contribute to the MPEs. In this case, single-period RC does not lead to sufficient performance, e.g., very slow convergence. With multiple repetitive controllers, i.e., multi-period RC, each repetitive controller corresponds with the fundamental frequencies present in the disturbance or reference signal. This potentially enables an increase in performance, as is investigated in this chapter.

First, a motivation for multi-period RC is given. It is shown that single-period RC may lead to unacceptable slow convergence. Second, various control architectures for multi-period RC are introduced, including the parallel and the so-called cascaded structure. Third, analysis of closed-loop systems is given to show that the cascaded structure has favorable properties for design and performance. Fourth, stability analysis is given to guarantee stability of the closed-loop systems. Fifth, the sequential design procedure for multi-period RC is presented. Furthermore, the sequential design procedure is discussed for the parallel structure, to show that this is a special case of the cascaded structure. Finally, simulations are performed to confirm the claims.

4.1 Motivation

Consider the following repetitive signals with different period lengths, i.e., $N_1 = 1f_s$, and $N_2 = 3.5f_s$.

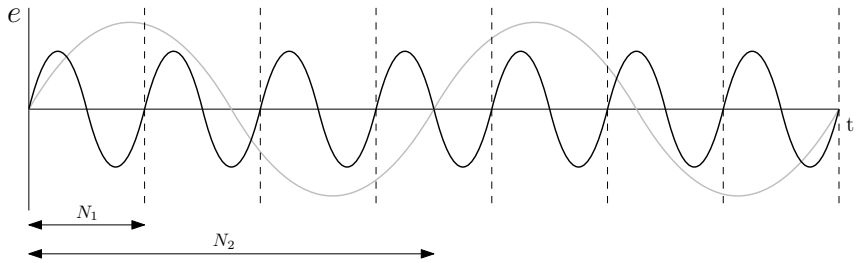

Figure 4.1: *Two repetitive signals with period lengths $N_1 = 1f_s$, and $N_2 = 3.5f_s$. Each vertical line indicates a period of f_s length.*

In many applications, many periodic disturbances are present, where the frequencies can be unrelated. Singe-period RC only achieves perfect disturbance rejection if the disturbance is periodic, assuming per-

fect model knowledge. For example in Figure 4.1, the disturbance is periodic with 7, i.e., the Least Common Multiple (LCM) of 1 and 3.5. For arbitrary real period lengths, the LCM may be very large. This is unacceptable in practice, since the memory and delay of the repetitive controller might grow very large, resulting in undesirable slow learning and large memory space.

Multi-period RC addresses multiple frequencies, which means that the periodic disturbances do not need to have an LCM to achieve disturbance rejection. Furthermore, in multi-period RC the memory length is reduced significantly, since this is a summation of each memory length of the repetitive controller. In Figure 4.1, the total memory length is $N_1+N_2 = 4.5f_s$. As a result, multi-period RC cannot only be implemented with a lower memory space than single-period RC, but also provide faster learning than single-period RC. This all motivates to elaborate further on multi-period RC.

4.2 Multi-Period Repetitive Control Setup

The aim of multi-period RC is to achieve perfect disturbance rejection or reference tracking for repetitive signals with multiple periods. Different structures for multi-period RC are known, which are the cascaded structure [15, 26], the parallel structure [6, 14, 16], and serial structure [14]. In this section, the parallel and cascaded structures are discussed, it is shown that parallel is a special case of cascaded. The serial structure is omitted in the present work, since convergence can be slow and it is hard to stabilize, see, e.g., [14].

The idea in multi-period RC is to include multiple controllers R_i in the control loop, for all $i = 1, 2, ..., n$, with n the number of individual repetitive controllers. Each individual repetitive controller has the same structure as discussed in Section 3.1, which is depicted in Figure 4.2.

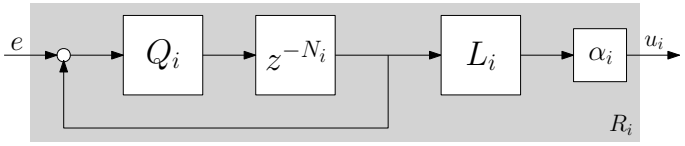

Figure 4.2: *Control scheme for each individual repetitive controller.*

The filters L and Q, period lengths N, and gains α may be chosen differently for each i,

$$R_i = (1 - z^{-N_i}Q_i)^{-1}\alpha_i L_i z^{-N_i} Q_i. \tag{4.1}$$

The key difficulty in multi-period RC is the design of each R_i structure. This is closely linked to the employed control structures discussed in the next section.

4.2.1 Parallel Memory Loops

Consider the control configuration of a discrete-time LTI SISO system, depicted in Figure 4.3, where the individual repetitive controllers are connected in parallel to the closed-loop feedback system.

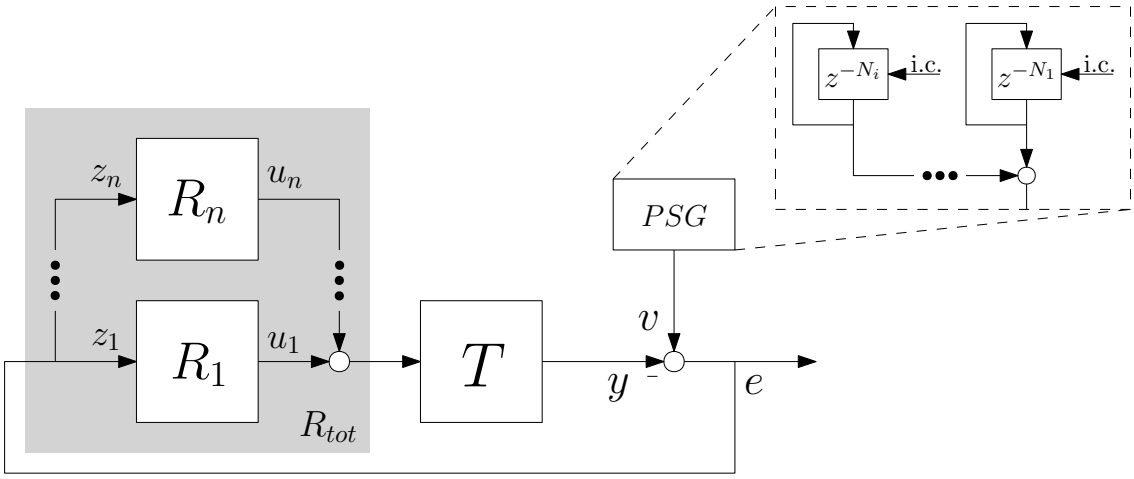

Figure 4.3: *Control configuration for multi-period RC in the parallel structure with a Periodic Signal Generator (PSG).*

With $T \in \mathcal{RH}_\infty$ as the complementary sensitivity, and $R_{tot} \in \mathcal{R}(z)$ as the total repetitive controller. The Periodic Signal Generator (PSG) block, highlighted in Figure 4.5, constructs signals with multiple frequencies according to the superposition principle, which states that the total repetitive signal is the summations of all N_i-periodic signals. The internal model of the multi-periodic disturbance is copied into the feedback loop by the parallel RC structure.

Now, let the error propagation $e = v - y$ be given by,

$$e = (1 + TR_{tot})^{-1} v = S_{R_{tot}} v, \tag{4.2}$$

with $S_{R_{tot}}$ as the modifying sensitivity. The total repetitive controller R_{tot} is a summation of the individual repetitive controllers, i.e.,

$$R_{tot} = \sum_{i}^{n} R_i, \tag{4.3}$$

for all $i = 1, 2, ..., n$.

Remark 4.1. Similar to single-period RC, also an add-on type repetitive controller configuration could be used, as shown in Figure 3.3. In this case, the error propagation is given by,

$$e = (1 + T(1 + R_{tot}))^{-1} v = S_{R_{tot}} S v. \tag{4.4}$$

However, the analysis and design choices are still based on $S_{R_{tot}}$, assuming $S \in \mathcal{RH}_\infty$.

An example of the modifying sensitivity function is given in Figure 4.4, with the disturbance frequencies as 50 Hz and 83 Hz, i.e., $N_1 = 20$ and $N_2 = 12$ respectively with sample frequency 1000 Hz. Here it is clearly visible, that the modifying sensitivity function consists of notches on each implemented frequency and all its higher harmonics, indicating disturbance rejection for multiple frequencies.

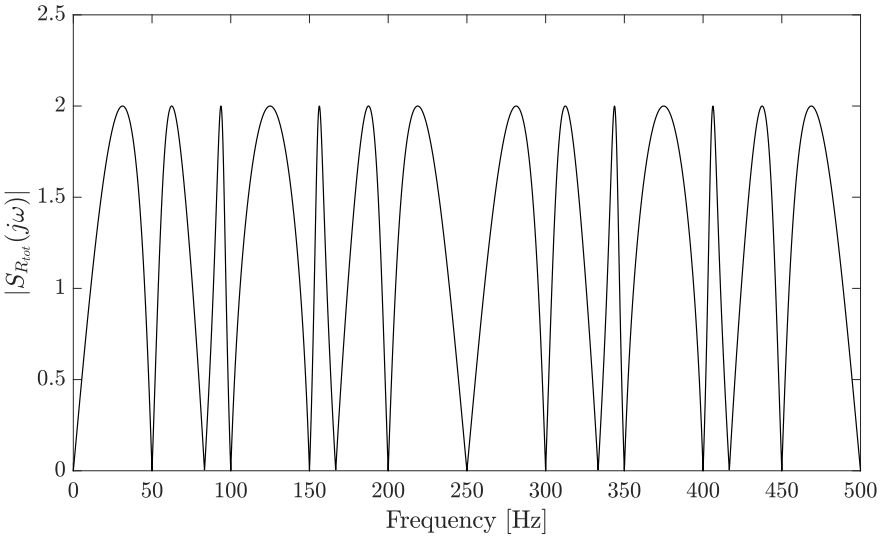

Figure 4.4: *Magnitude of the modifying sensitivity function. The period lengths are $N_1 = 20$ and $N_2 = 12$ respectively, the robustness filter is chosen as $Q_i = 1$, and learning gains as $\alpha_1 = \alpha_2 = 0.5$, and $L_i = T^{-1}$.*

Remark 4.2. In this particular example, the total memory length is 32, where the LCM is 60. This confirms the potential of multi-period RC, regarding the memory space, in comparison with single-period RC.

4.2.2 Cascaded Memory Loops

Next, the cascaded structure is presented, where $\hat{T} \in \mathcal{RH}_\infty(z)$ is added as the parametric model of T.

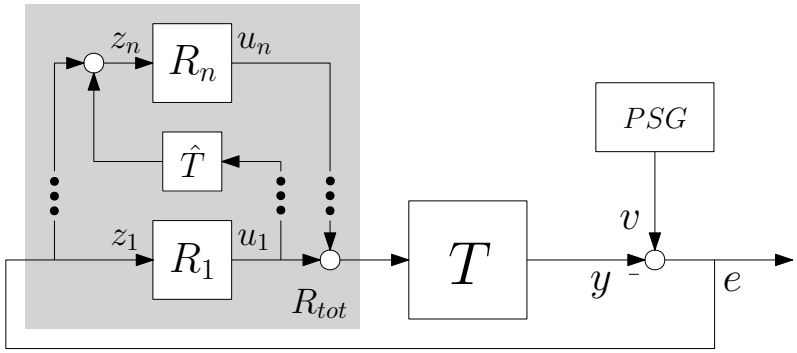

Figure 4.5: *Control configuration for multi-period RC in the cascaded structure with a Periodic Signal Generator (PSG).*

Interpretation of the cascaded structure, i.e., the effect of including model $\hat{T}$, is as follows. Each individual repetitive controller R_i, tries to reduces the error signal e. However, the control effort of R_i is hidden for R_{i+1}, by reconstructing the effect of R_i on T through the plant model $\hat{T}$. This reconstruction is then added to the original error signal, which ensures that R_i only suppresses the corresponding repetitive signal with period length N_i, in case of $\hat{T} = T$. The remaining error is then left for the other repetitive controller to suppress. As a result, the repetitive controllers do not react to each others control efforts.

Similar to (4.2), the modifying sensitivity function is given by,

$$S_{R_{tot}} = (1 + TR_{tot})^{-1}. \tag{4.5}$$

Except, now the total repetitive controller is obtained as,

$$R_{tot,i} = R_{tot,i-1} + R_i(1 + \hat{T}R_{tot,i-1}), \tag{4.6}$$

with $R_{tot} = R_{tot,n}$ and $R_{tot,0} = 0$, for all $i = 1, 2, ..., n$.

Example 4.1. If $n = 2$, then the total repetitive controller is given by,

$$R_{tot,1} = 0 + R_1(1 + \hat{T} \cdot 0) = R_1, \tag{4.7}$$

$$R_{tot,2} = R_{tot,1} + R_2(1 + \hat{T}R_{tot,1}) = R_1 + R_2(1 + \hat{T}R_1), \tag{4.8}$$

resulting in $R_{tot} = R_{tot,2}$.

Design and stability conditions of each individual repetitive controller in a multi-period RC setting are not straightforward, especially with respect to model errors. The total repetitive controller R_{tot} consists of interactions between each individual repetitive controller, depending on the model error $\hat{T} \neq T$. Independent SISO design for each repetitive controller, i.e., (3.16), might lead to an unstable system, since the interactions are ignored. Hence, analysis of the closed-loop system is presented next to deal with this interaction component.

4.3 Analysis of Closed-Loop System

In this section, the analysis of the closed-loop system for multi-period RC in the cascaded structure is presented, which is key in understanding the multi-period RC sequential design approach. Recall that the closed-loop is just given by the modifying sensitivity function, in case of the control configuration depicted in Figure 4.5. First, the analysis is presented, where after it is supported by an example.

The modifying sensitivity function (4.5) can be rewritten as the product of sensitivities with each having a different equivalent plant T_{i-1}^{eq} and repetitive controller R_i, i.e.,

$$S_{R_{tot}} = (1 + TR_{tot})^{-1} = \prod_{i}^{n}(1 + T_{i-1}^{eq}R_i)^{-1}, \tag{4.9}$$

with R_i as in (4.1). Each individual sensitivity function corresponds to the loop gain of each individual repetitive controller. The equivalent plant is the transfer function from u_n to z_n, depicted in Figure 4.5, i.e., what the repetitive controller 'sees' as plant to be controlled. The equivalent plant is given by,

$$T_i^{eq} = (1 + T_{i-1}^{eq}R_i)^{-1}T_{i-1}^{eq}(1 + \hat{T}R_i), \tag{4.10}$$

with $T_0^{eq} = T$, for all $i = 1, 2, ..., n - 1$. Each equivalent plant T_i^{eq} includes all preceding repetitive controllers $R_1, ..., R_i$. The equivalent plant in (4.10) is given in a recursive form, the derivation is given in Appendix A.

The modifying sensitivity function $S_{R_{tot}}$ is the product of sequentially dependent factors. This motivates the sequential design approach, presented in Section 4.5. Note that the sequential dependency is only obtained if $\hat{T} \neq T$, i.e., if $\hat{T} = T$ then $T_i^{eq} = T$, $\forall i$.

If $\hat{T} = T$, then each repetitive controller is decoupled, i.e.,

$$S_{R_{tot}} = \prod_{i}^{n}(1 + TR_i)^{-1}. \tag{4.11}$$

This motivates why the cascaded structure is powerful in handling the interactions between each repetitive controller. Now, each repetitive controller can be designed independently, meaning that the settling time of the total repetitive controller is completely decoupled into the summations of the individual settling times [26].

The results given in (4.9) and (4.10) are obtained from a recursive approach, given in Appendix A. Therefore, it is visualized in the next section for the case $n = 2$ to gain more insight.

4.3.1 Example: Two Cascaded Repetitive Controllers

The objective of this example is to illustrate (4.9) and (4.10) for $n = 1$ and $n = 2$. First, consider $n = 1$, i.e., single-period RC. The control configuration is depicted in Figure 4.6 on the left hand-side, together with a corresponding standard plant representation on the right hand-side.

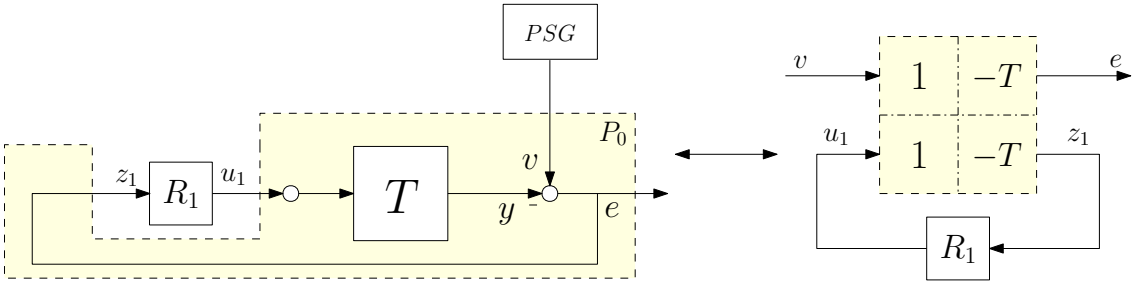

Figure 4.6: *Left: Control configuration for single-period RC with R_1. Right: Standard plant representation.*

The dotted yellow block, depicted by P_0, is the transformation matrix between the defined in- and outputs of the standard plant. The defined inputs are, the disturbance v and output of the repetitive controller u_1. The outputs are, the error signal e and the input z_1 for the repetitive controller.

The control objective of this standard plant representation is to design R_1 such that the closed-loop system, i.e., the transfer from v to e, is stable. The closed-loop transfer function from v to e is obtained by taking the lower Linear Fractional Transformation (LFT) of P_0 with respect to R_1, i.e.,

$$S_R = F_l(P_0, R_1) = 1 - TR_1(1 + TR_1)^{-1}, \tag{4.12}$$

$$= (1 + TR_1)^{-1}, \tag{4.13}$$

which is also known as the modifying sensitivity function S_R. The plant seen by R_1 is given by the lower right corner of P_0, i.e., the transfer from u_1 to z_1, which is $-T$. Notice that these are all familiar results from single-period RC.

Now, consider multi-period RC, i.e., take $n = 2$. The control configuration is depicted in Figure 4.7 on the left hand-side, together with the corresponding standard plant representation on the right hand-side, assuming that the loop gain of R_1 is closed.

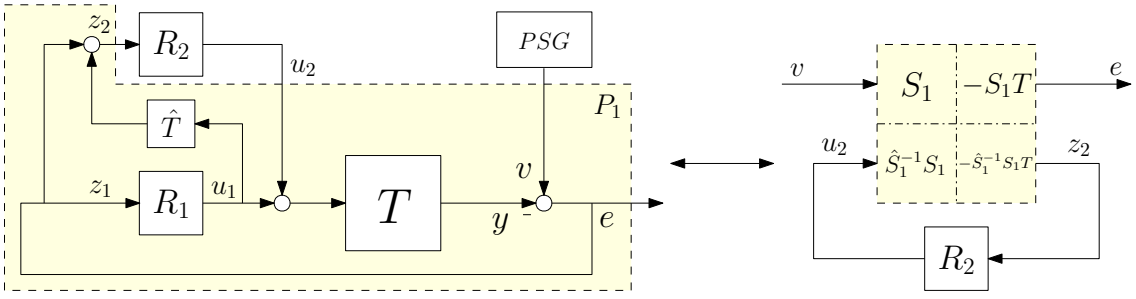

Figure 4.7: *Left: Control configuration for multi-period RC with R_1 and R_2 in the cascaded structure. Right: Standard plant representation.*

The same methodology is used for R_2, which means that R_2 is designed by the lower LFT of P_1 with

respect to R_2. Now, the closed-loop transfer function $S_{R_{tot}}$, i.e., the transfer from v to e, is given by,

$$\begin{aligned} S_{R_{tot}} &= F_l(P_1, R_2) = S_1 - S_1 T R_1 (1 + \hat{S}_1^{-1} S_1 T R_1)^{-1} + \hat{S}_1^{-1} S_1, \qquad (4.14) \\ &= S_1 (1 + \hat{S}_1^{-1} S_1 T R_2)^{-1}, \\ &= (1 + TR_1)^{-1} (1 + \underbrace{(1 + TR_1)^{-1} (1 + \hat{T} R_1) T}_{T_1^{eq}} R_2)^{-1}. \qquad (4.15) \end{aligned}$$

with $S_1 = (1 + TR_1)^{-1}$, and $\hat{S}_1^{-1} = (1 + \hat{T} R_1)$.

Remark 4.3. Generic expressions for S_{n-1} and $\hat{S}_{n-1}^{-1}$ are given in Appendix A. Note that for $n = 1$, $S_0 = 1$ and $\hat{S}_0^{-1} = 1$.

Clearly, this modifying sensitivity function (4.15) is the product of the first sensitivity for R_1 and the second sensitivity for R_2 with the equivalent plant containing all the interaction components. Notice that R_1 must be designed in order to design R_2. This motivates a sequential design approach, i.e., design each repetitive controller based on the previously designed ones.

Remark 4.4. Notice that if $\hat{T} = T$, then $T_1^{eq} = T$ in (4.15). Indicating two completely decoupled sensitivity functions.

4.4 Stability Analysis

The analysis of the closed-loop system in Section 4.3 showed that $S_{R_{tot}}$ is the product of sequentially dependent factors. In this section, this sequential structure is exploited in view of stability analysis.

Stability of the closed-loop system, depicted in Figure 4.5, with n repetitive controllers in the cascaded structure, can be verified as follows. Let $H_i(z) = (1 - \alpha_i T_{i-1}^{eq} L_i) z^{-N_i} Q_i$.

Theorem 4.1 (Nyquist stability theorem for sequential design of multi-period RC)**.** *Consider the control configuration in Figure 4.5, with R_i as in* (4.1)*, suppose all poles of $\hat{T}$, L_i, Q_i, and T_{i-1}^{eq} as in* (4.10) *are on the open unit disc, and assume no unstable pole-zero cancellations between $(1 - z^{-N_i} Q_i)$ and $(1 - H_i(z))$ in* (4.9)*. Then the closed-loop system* (4.9) *is stable if and only if the image of $(1 - \alpha_i T_{i-1}^{eq} L_i) z^{-N_i} Q_i$, for all $i = 1, 2, ..., n$,*

1. *makes no encirclements of the point $1 + 0j$, and*
2. *does not pass through the point $1 + 0j$,*

as z goes around the Nyquist contour Γ in Figure 3.11.

Proof. Factorization of (4.9), with the repetitive controller as in (4.1), yields the following derivation,

$$S_{R_{tot}} = \prod_i^n (1 - z^{-N_i} Q_i) \prod_i^n \left(1 - (1 - \alpha_i T_{i-1}^{eq} L_i) z^{-N_i} Q_i\right)^{-1}. \qquad (4.16)$$

The Nyquist stability criterion can be used on the products on the right hand-side of (4.16), with $(1 - H_i(z))$ as the return difference and $H_i(z)$ as the loop gain. Assuming that $(1 - z^{-N_i} Q_i)$ and $(1 - H_i(z))$ do not imply unstable pole-zero cancellations for all $i = 1, 2, ..., n$ and all cross products for $i > 1$.

Furthermore, Theorem 4.1 states that all poles of T_{i-1}^{eq}, L_i,Q_i, and $\hat{T}$ should lie on the open unit disc. This can be achieved easily for every L_i- and Q_i-filter, and $\hat{T}$, since those are design choices. However, the resulting equivalent plant T_{i-1}^{eq} has to be checked. Note that the equivalent plant (4.10) can be written as (A.5), i.e.,

$$T_{n-1}^{eq} = \hat{S}_{n-1}^{-1} S_{n-1} T, \tag{4.17}$$

$$= \prod_{i}^{n} \big[(1 - z^{-N_i} Q_i)^{-1} \big(1 - (1 - \alpha_i \hat{T} L_i) z^{-N_i} Q_i\big)(1 - z^{-N_i} Q_i) \big(1 - (1 - \alpha_i T_{i-1}^{eq} L_i) z^{-N_i} Q_i\big)^{-1}\big] T,$$

$$= \prod_{i}^{n} [\underbrace{\big(1 - (1 - \alpha_i \hat{T} L_i) z^{-N_i} Q_i\big)}_{1} \underbrace{\big(1 - (1 - \alpha_i T_{i-1}^{eq} L_i) z^{-N_i} Q_i\big)^{-1}}_{2})] T. \tag{4.18}$$

Consider the following observations.

1. Term 1 in (4.18) is stable, since Q_i, L_i, and $\hat{T}$ are stable.
2. Term 2 in (4.18) is stable, due to preceding designs.
3. T is assumed to be stable.

Consequently, T_{i-1}^{eq} is stable for all $i = 1, 2, ..., n$. □

Although Theorem 4.1 provides a necessary and sufficient stability condition for multi-period RC, it is inconvenient for design purposes. Furthermore, if a different N is implemented, then it does not guarantee stability. This motivates the following Lemma.

Lemma 4.2. *Under assumption of Theorem 3.2 and $H_i(z)$ is strictly proper, the closed-loop system* (4.9) *with R_i as in* (4.1) *is stable for all $N \in \mathbb{N}$ if*

$$|(1 - \alpha_i T_{i-1}^{eq}(e^{j\omega}) L_i(e^{j\omega})) Q_i(e^{j\omega})| < 1 \quad \forall i \quad \forall \omega \in [0, \pi]. \tag{4.19}$$

Proof of Lemma 4.2 is equivalent with the proof of Lemma 3.3 given in Section 3.3. According to (4.19), every loop can now be designed as a SISO design problem. Each of which is sequentially dependent on each other. In this way, interaction is explicitly accounted for, since T^{eq} contains all preceding repetitive controllers and modeling errors. Hence, the following sequential design procedure is established.

4.5 Sequential Design Procedure

In this section, a sequential design procedure is given for multi-period RC. It is shown how sequential design for multiple repetitive controllers results in generic design conditions for each individual repetitive controller. Sequential design is commonly done in practice for feedback control [13, 17, 21], yet its potential for RC is unexplored.

In multi-period RC, the repetitive controllers are connected with other repetitive controllers, indicating that interaction between the controllers is unavoidable. By means of sequential designing, the repetitive controllers can be designed explicitly for interaction from preceding loops. Starting with designing the first repetitive controller, i.e., single-period RC, and consequently closing this loop. Then, design the next repetitive controller based on an equivalent plant, which includes all interaction from preceding loops, and continue this procedure. In this way, each of the repetitive controllers explicitly accounts for modeling errors in the previously designed loops.

The loop-closing order is an important factor, since it affects the resulting closed-loop system, and it determines performance due to previously designed loops. Iterative redesigns may hence be required, until the total design satisfies the requirements, resulting in the following sequential design procedure.

Procedure 4.1 Frequency-domain multi-period RC sequential design

Given a nonparametric model of T, perform the following sequence of steps.

1. Construct parametric model $\hat{T}(z)$ according to T, and design $L_i(z) = \hat{T}^{-1}(z)$ for all i.
2. Choose the order in which the loops are designed.
3. Set the index $i = 1$, and perform the following steps.
   (a) Construct T_{i-1}^{eq} according to (4.10).
   (b) Given $L_i(z)$ and T_{i-1}^{eq}, design Q_i and α_i according to (4.19) in Lemma 4.2.
   (c) Until $i = n$, set $i = i + 1$ and return to step 3a.
   (d) If the resulting closed-loop system is unsatisfactory, reset $i = 1$, return to step 3a.
4. If the closed-loop system is unsatisfactory after iterations, return to 2. and change design order.

Procedure 4.1 has the following implications for design of L_i,Q_i, and α_i for the cascaded structure.

4.5.1 Learning Filter

In Procedure 4.1, it is proposed to construct the learning filter based on parametric model $\hat{T}$, i.e., $L_i = \hat{T}^{-1}$ for all $i = 1, 2, ..., n$. Notice however that (4.19) would suggest to design the learning filter based on T_{i-1}^{eq}, instead of $\hat{T}$. This choice is motivated next.

Parametric models of T_{i-1}^{eq} might be difficult to obtain, since

1. the model might result in high order, due to the modeling error $\hat{T} \neq T$, and
2. this equivalent plant might have non-minimum phase zeros depending on the previous robustness filters Q_i.

Hence, the learning filter is recommended to be kept the same for each repetitive controller, i.e., $L_i = \hat{T}^{-1}$ for all $i = 1, 2, ..., n$. This is valid as long as $T_i^{eq} \approx T \, \forall i$, which is true for the cascaded structure if,

- $\hat{T} = T$, i.e., no modeling errors, then $T_i^{eq} = T \, \forall i$, and
- if $\hat{T} \neq T$, then
  - term 1 in (4.18) equals 1, if $L = \hat{T}^{-1}$ and $\alpha_i = 1$, and
  - term 2 in (4.18) is (approximately) 1, if (4.19) is small,

  resulting in $T_i^{eq} \approx T \, \forall i$, illustrated in Section 4.7.

This makes the sequential design approaches powerful, since no modeling errors are lost in the formulations and designs choices. The non-causal learning filters are implemented as shown in Figure 3.12.

4.5.2 Robustness Filter

In the sequential design approach, the robustness filter is a key component to improve performance. Not only is the robustness filter used for modeling errors $\hat{T} \neq T$, but also for the deliberately introduced mismatch of $L_i \neq (T_{i-1}^{eq})^{-1}$ for $i > 1$. Notice that the introduced mismatch is typically small due to previous designs, see Section 4.5.1. Thus, each robustness filter can explicitly be designed based on previously designed repetitive controllers indicating that conservatism is reduced. Non-causal robustness filters are implemented as shown in Figure 3.12.

4.5.3 Learning Gain

According to (4.19), the learning gain should be chosen as $0 < \alpha_i < 2$. Properties are discussed in Section 3.4.3.

4.5.4 Connections to Existing Approaches for Cascaded Structure

In [26], interaction from other loops is treated as uncertainty, and dealt with through conservative robust design. This means that only one robustness filter would be designed based on $\hat{T}$. In comparison, the sequential design approach explicitly accounts for these interactions in the design, since often in practice they are accurately known, assuming an accurate FRF measurement. This potentially reduces conservatism and improves performance.

4.6 Special Case: Sequential Design for Parallel Structure

In this section, the developed sequential design approach is applied to a parallel RC structure. The parallel structure is a special case of the cascaded structure, in the sense that the block $\hat{T}$ is removed from the cascaded RC control structure, compare 4.3 and 4.5. Hence, the control effort from preceding repetitive controllers R_i is not hidden for R_{i+1} for all $i = 1, 2, ..., n$.

Consider the same control configuration as 4.3, with the equivalent standard plant representation on the right hand-side, depicted in Figure 4.8. Recall that the definition of S_{n-1} is given in Appendix A.

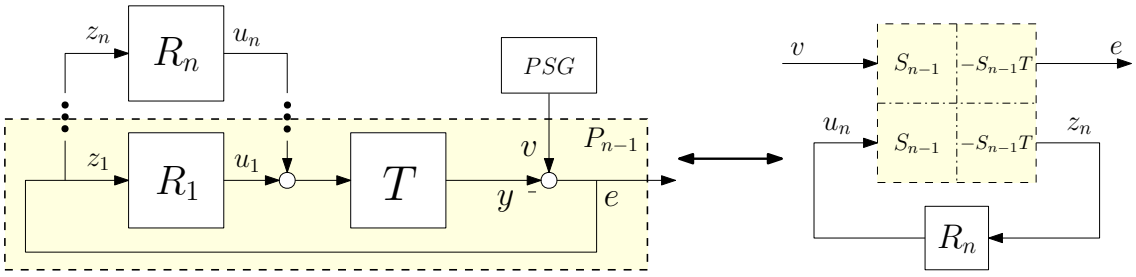

Figure 4.8: *Left: Control configuration for multi-period RC in parallel structure, Right: Standard plant representation.*

All results from Sections 4.3 till 4.5 can be applied here as well, only without the presence of $\hat{T}$ in the control structure. The equivalent plant is now given by,

$$T_{n-1}^{eq} = S_{n-1}T, \tag{4.20}$$

or in a recursive form as,

$$T_i^{eq} = (1 + T_{i-1}^{eq} R_i)^{-1} T_{i-1}^{eq}, \tag{4.21}$$

with $T_0^{eq} = T$, for all $i = 1, 2, ..., n-1$. Comparing (4.21) with (4.10), i.e., the equivalent plant for the parallel structure, shows that the term $(1 + \hat{T}R_i)$ is absent. This implies that T^{eq} may significantly deviate from T, which complicates filter designs. This is addressed in the next subsection.

4.6.1 Filter Design

Procedure 4.1 can be used in the parallel structure, however the contribution of the filters and gains is much more involved, especially the robustness filter and learning gain. According to (4.20) and (4.21), T^{eq} may significantly deviate from T, since the open-loop unstable poles are not canceled by $\hat{S}_{n-1}$, i.e., $\hat{T}$ is not present in the parallel structure. Therefore, designing the learning filters as $L_i = (T_{i-1}^{eq})^{-1}$ is not suitable, since parametric model of T_{i-1}^{eq} might be difficult to obtain. In addition to issues 1 and 2 in Section 4.5.1, a third issues is defined:

3. the delay terms z^{-N_i} in the previous repetitive controllers might lead to very high order of T_{i-1}^{eq}.

Hence, the learning filters are still kept the same for each repetitive controller, i.e., $L_i = \hat{T}^{-1}$.

Now, the robustness filter addresses the model mismatch $\hat{T} \neq T$ and $L_i \neq (T_{i-1}^{eq})^{-1}$ for $i > 1$, which is similar to the cascaded structure. However, since the deviation of T_{i-1}^{eq} and T for $i > 1$ is much more than in the cascaded structure, due to 1,2, and 3, explicitly designing the robustness filter is possibly not enough, illustrated in Section 5.2.1.

4.6.2 Connections to Existing Approaches

In [16], it is suggested that the learning gain for the parallel structure should satisfy the following theorem.

Theorem 4.3. *Assume that the individual RC loops are stable, i.e.,*

$$|(1 - \alpha_i T(e^{j\omega})L(e^{j\omega}))Q^n(e^{j\omega})| < 1 \quad \forall i \quad \forall \omega \in [0, \pi], \tag{4.22}$$

then the overall closed-loop system shown in Figure 4.3 is asymptotically stable if the control gains α_i, satisfy the following inequality for all $i = 1, 2, ..., n$.

$$0 < \sum_{i=1}^{n} \alpha_i < 2. \tag{4.23}$$

In [16], the filters are designed independently, i.e., the same filters are obtained for each loop with the learning gains satisfying Theorem 4.3. The price that is paid for this simple design is that the learning gains have to be chosen small, see (4.23). This typically results in slow learning of the closed-loop system, which may be undesirable. This is in contrast with the sequential design procedure, where the learning filter and robustness filter can explicitly be designed for interaction from previously design RC loops. As a key difference, the sequential design procedure allows for the learning gain $\alpha_i = 1 \, \forall i$, which potentially improves performance.

4.7 Simulations: Sequential Design Procedure

In this section, simulations are performed to validate the standard design procedure, i.e., Procedure 3.1, and the sequential design procedure, i.e., Procedure 4.1. The resulting designs choices are presented in Table 4.1. In Chapter 5, these design procedures are investigated in more detail for the experimental setup. For simulations, the comparison is made between one memory loop (single-period RC), and two memory loops, respectively the parallel and cascaded structures (multi-period RC). The simulations serve to

- illustrate the benefit of multiple memory loops,
- illustrate the interaction in the parallel structure, and
- compare the convergence speed of the three different structures.

4.7.1 Disturbance Signal

The disturbance signal used in simulations is depicted in Figure 4.9. This signal corresponds to the real disturbance, as described in Section 2.1. The grey areas indicate where the printing takes place. Furthermore, each print-pass is defined by $N = 1000$ samples and the sampling time is 0.001 $[s]$. This disturbance signal consists of,

- a sine wave of period length $N_1 = 143$ samples, i.e., ≈ 7 Hz. With amplitude 0.01 $[mm]$, and
- a fourth-order forward-backward signal with two positive and two negative steps. Each step is 0.1 $[mm]$ and the length is one print-pass, i.e., this signal is periodic with $N_2 = 4000$ samples.

The LCM of these two signals is $N_l = 572000$, i.e., 572 $[s]$.

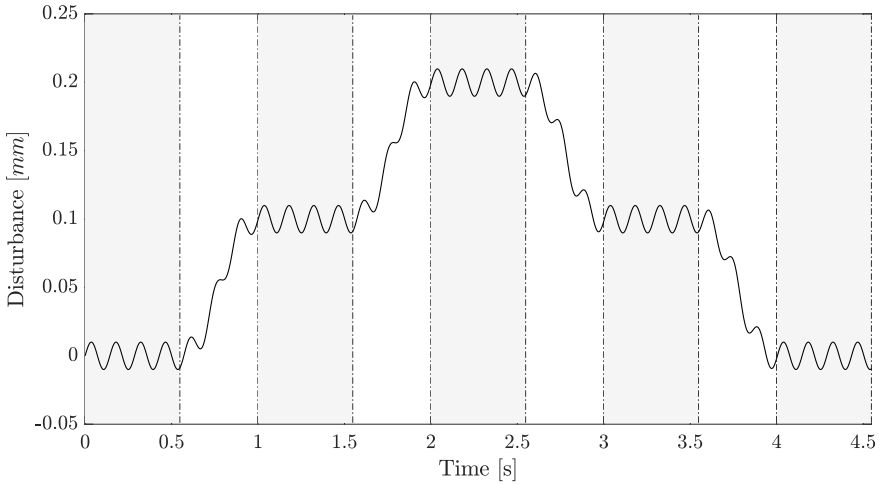

Figure 4.9: *The disturbance signal for simulations, consisting of a four-order forward-backward signal and a sine wave.*

The two different period lengths are used in the parallel and cascaded structure, i.e., $N_1 = 143$ and $N_2 = 4000$. For single-period RC, the LCM is used, i.e., $N_l = 572000$.

4.7.2 Parametric Models

The design procedures requires a parametric model of the system T, which is described by the complementary sensitivity function $T(z)$ consisting of a plant model $G(z)$, and a stabilizing feedback controller $K(z)$. Both $G(z)$ and $K(z)$ are given in Section 2.3. For simulations purposes, a plant model $\hat{G}(z)$ is designed, to simulate the modeling error. This plant model $\hat{G}(z)$ is based on the same system, however with less damping. The same feedback controller $K(z)$ is used, resulting in $\hat{T}(z)$. The Bode diagram of the models $T(z)$ and $\hat{T}(z)$ are given in Figures 4.10 and 4.11.

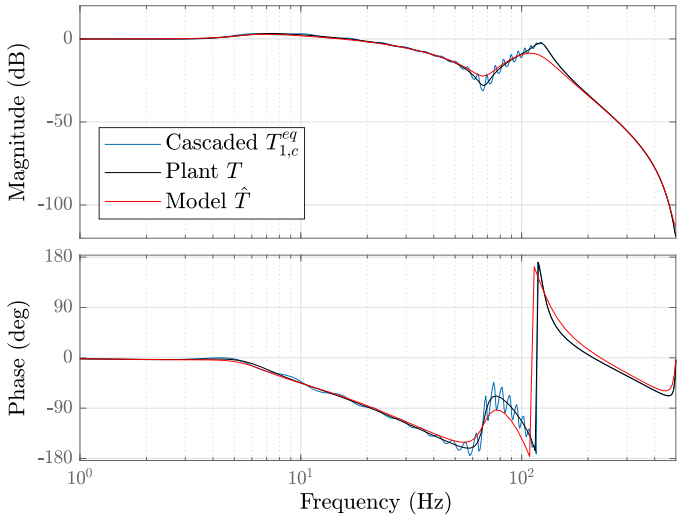

Figure 4.10: *Bode diagram of T, $\hat{T}$, and $T_{1,c}^{eq}$ for the cascaded structure.*

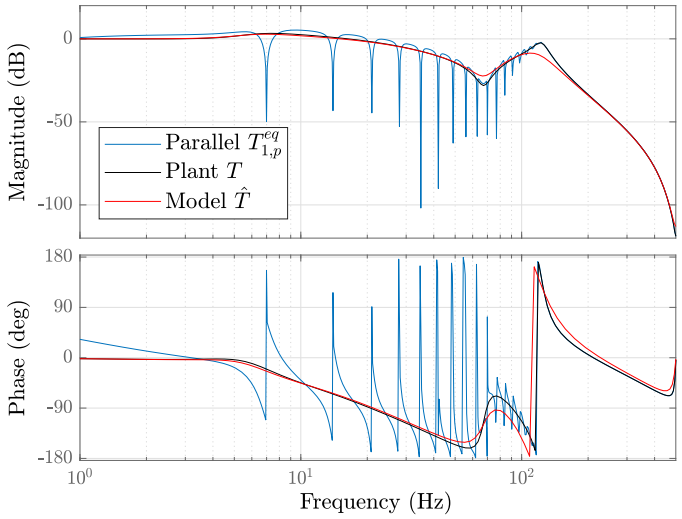

Figure 4.11: *Bode diagram of T, $\hat{T}$, and $T_{1,p}^{eq}$ for the parallel structure.*

Two memory loops implies one equivalent plant, for both the cascaded and parallel structure. The equivalent plants are depicted in Figures 4.10 and 4.11, respectively.

- The cascaded equivalent plant, depicted in Figure 4.10, is very similar to the original plant. Only minor mismatch is obtained, since the effect of the preceding repetitive is not entirely canceled in 4.10 due to the simulated modeling error, i.e., $\hat{T} \neq T$.
- This is in contrast with the parallel structure, depicted in Figure 4.11, where the notches on 7 Hz and all higher harmonics are present in the equivalent plant. They are not canceled in (4.20), since $\hat{T}$ is not present in the parallel structure. This already indicates the amount of interaction in the second repetitive controller.

For both equivalent plants, it is clearly visible that the first robustness filter, given in Table 4.1, determines the frequencies until $T_1^{eq} \neq T$, in this case 110 Hz.

The design choices for each individual repetitive controller are given in Table 4.1, with $f_{c,i}$ the cut-off frequency for each robustness filter. The robustness filters are designed as a 50th order zero-phase low-pass FIR filter. Both learning filters are designed through stable inversion of $\hat{T}$ by the ZEPTC algorithm.

Table 4.1: *Repetitive controller designs.*

	$f_{c,1}$ [Hz]	$f_{c,2}$ [Hz]	α_1 [-]	α_2 [-]
Single-period RC design (Procedure 3.1)	110	–	1	–
Sequential design: Parallel (Procedure 4.1)	110	90	0.5	0.5
Sequential design: Cascaded (Procedure 4.1)	110	90	1	1

Remark 4.5. The differences between the cut-off frequencies and the learning gains are explained in Chapter 5.

4.7.3 Tracking Error

The tracking errors for single-period RC, parallel RC, and cascaded RC are depicted in Figure 4.12, together with the disturbance signal. The system is simulated for 580 print-passes. In Figure 4.13 the normalized 2-norm of the disturbance, single-period RC, parallel RC, and cascaded RC are depicted. The convergence speed is normalized over one period N_1. The corresponding print-passes are depicted at the top x-axis.

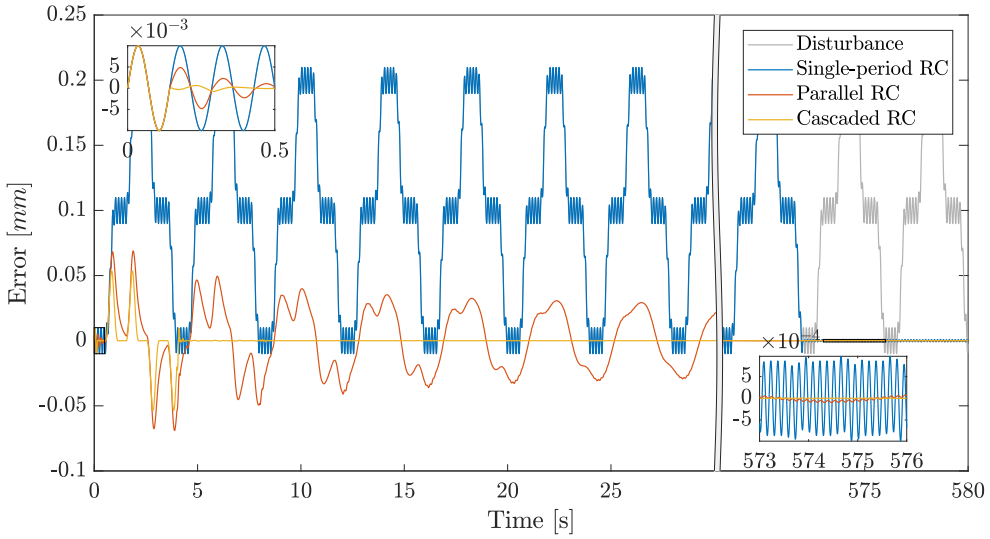

Figure 4.12: *Comparison of the disturbance, and the tracking error for single-period RC, parallel RC, and cascaded RC as function of time [s]. The figure is compressed to demonstrate the final tracking error. The left zoom plot shows the early learning behavior of multi-period RC. The right zoom plot shows the remaining error after 573 [s].*

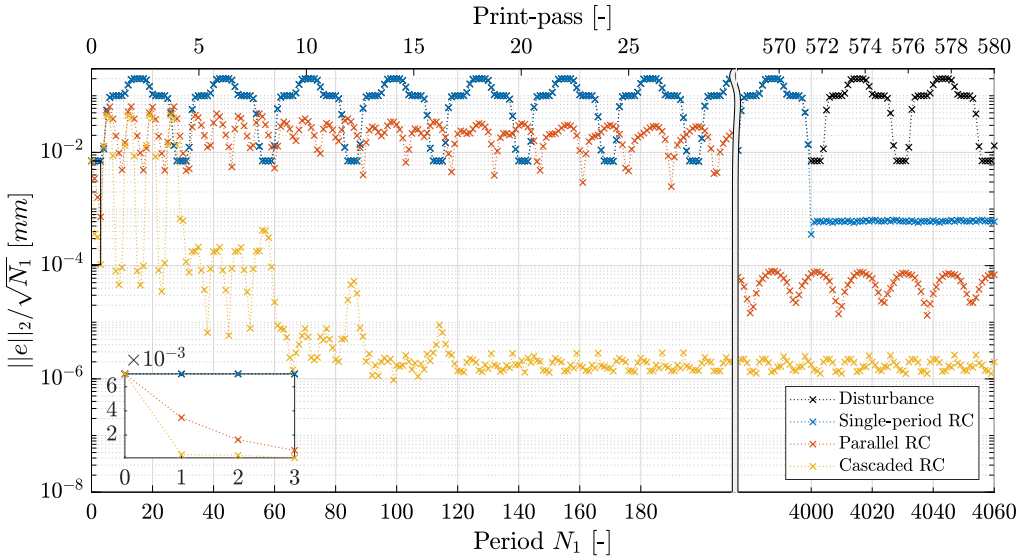

Figure 4.13: *Comparison of the normalized 2-norm of the disturbance, and the tracking error for single-period RC, parallel RC, and cascaded RC as function of the period N_1. The top axis shows the corresponding print-passes. This figure is compressed to demonstrate the slow convergence speed of parallel RC and single-period RC. The left zoom plot shows early learning behavior of multi-period RC.*

From Figure 4.12, it is clearly visible that each RC structure reduces the tracking error. However, some different observations can be made regarding the structures.

- First, single-period RC achieves disturbance rejection for period length $N_l = 572000$ samples, i.e., after 572 print-passes. The error is not perfectly rejected due to $\hat{T} \neq T$, depicted in the right zoom plot of Figure 4.12. It takes a few RC updates to achieve the asymptotic error, with this modeling error. Hence, single-period RC results in very slow convergence, which confirms the benefit of multiple memory loops.
- The parallel structure starts to learn after $N_1 = 147$ samples, depicted in the left zoom plot in Figure 4.12. However, the interaction between the individual repetitive controllers in the parallel structure results in very slow convergence, demonstrated in Section 4.7.4. The tracking error is still not converged after 580 $[s]$.
- The cascaded structure also learns after $N_1 = 147$ samples. Including the parametric model $\hat{T}$ reduces the interaction significantly, resulting in fast convergence. The tracking error is (approximately) zero after ≈ 4 print-passes.

Figure 4.13 shows that in 580 print-passes.

- The tracking error is reduced from roughly $\mathcal{O}(10^{-1})$ to $\mathcal{O}(10^{-4})$, and to $\mathcal{O}(10^{-3})$ after 572 print-passes for parallel RC and single-period RC, respectively. Confirming the slow convergence of single-period RC and parallel RC.
- The tracking error is reduced from roughly $\mathcal{O}(10^{-1})$ to $\mathcal{O}(10^{-6})$ after 17 print-passes for the cascaded structure. The asymptotic error is achieved in four RC updates due to the modeling error.

4.7.4 Interaction Analysis

The best way to understand the interaction between the individual repetitive controller in both structures, and the effect of the parametric model $\hat{T}$ in the cascaded structure, is to simulate the process. In Figure 4.14, the disturbance and the tracking errors seen by each individual repetitive controller for the parallel structure and cascaded structure are depicted. Recall, these input signal are defined as z_1 and z_2 in Figures 4.3 and 4.5.

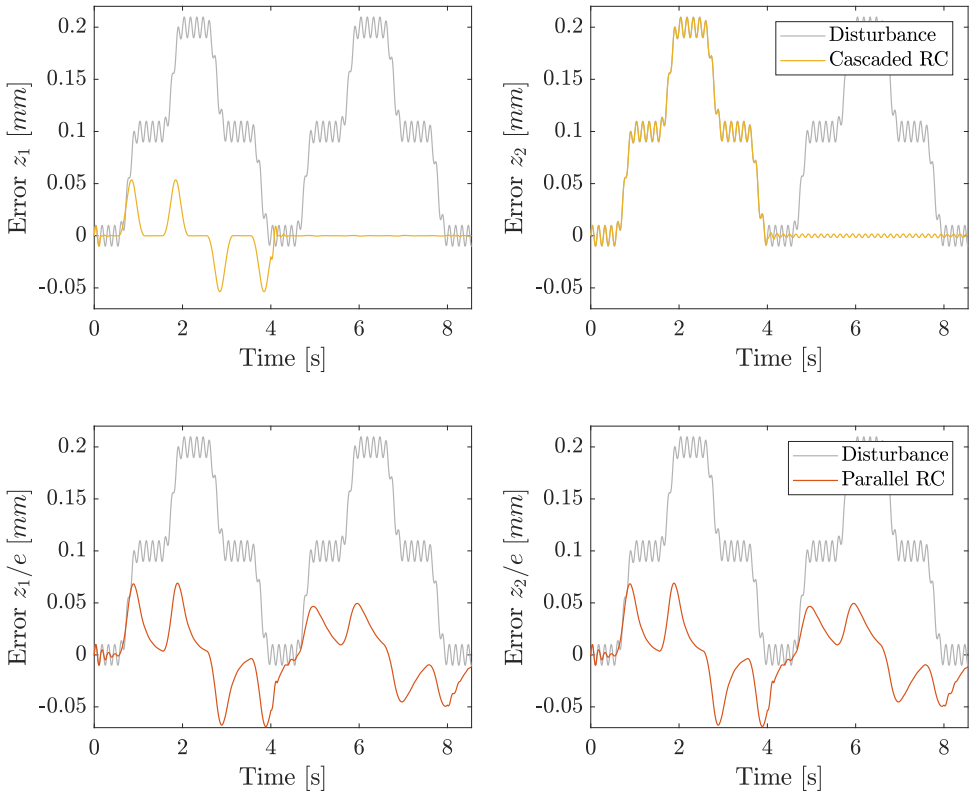

Figure 4.14: *The disturbance and tracking error seen by the individual repetitive controllers in parallel RC and cascaded RC are depicted. The top left figure shows z_1, and the top right z_2, for cascaded RC, i.e., depicted in Figure 4.5. The bottom figures shows the error signal, i.e., z_1 and z_2 in Figure 4.3, for parallel RC, which are equivalent.*

The following observations are made regarding the interaction between the two individual repetitive controllers.

- In parallel RC, i.e., bottom two figures, the control effort of the repetitive controller acting on $N_1 = 147$ is clearly visible in $0-4$ [s]. The shortest period length $N_1 = 147$ samples is rejected within the a couple short period lengths. Afterwards, this repetitive controller is basically acting as an integrator, meaning that the constant part of the disturbance signal is suppressed, resulting in the shark teeth. Hence, the input signal (z_2) for the repetitive controller acting on $N_2 = 4000$ samples, depicted in the lower right corner of Figure 4.14, is disturbed by the repetitive controller acting on $N_1 = 147$ samples, i.e., this signal is not periodic with $N_2 = 4000$ samples. This interaction between the individual repetitive controllers in the parallel structure results in slow convergence.
- In case of cascaded RC, the control effort of the repetitive controller acting on $N_1 = 147$ samples is still present in z_1, depicted in the top left corner in Figure 4.14. However, this control effort is hidden from the repetitive controller acting on $N_2 = 4000$ samples, by including the model $\hat{T}$ in the structure. Therefore, the input signal (z_2) for this repetitive controller, depicted in the top right corner of Figure 4.14, is just the disturbance signal. This results in fast convergence, since this signal is periodic with $N_2 = 4000$.

Consequently, the cascaded structure show promising results regarding interaction reduction between the individual repetitive controllers and fast convergence speed. In the next chapter, this is investigated on the experimental setup.

Chapter 5

Experimental Application to a Wide-Format Roll-To-Roll Printing System

In this chapter, the developed theoretical framework for multi-period RC design is experimentally validated on the wide-format Roll-To-Roll (RTR) printing system, as introduced in Chapter 2. The experimental results confirm that,

- the sequential design procedure results to be less conservative and increases the performance, compared to pre-existing design approaches [16, 26],
- the multi-period RC framework achieves rejection of exogenous disturbances consisting of multiple unrelated periods, and
- the cascaded structure gives most promising results, with respect to reducing interaction, convergence speed, and asymptotic performance.

The outline of this chapter is as follows. First, two case studies are presented, to validate the developed theory. Second, multi-period RC designs are made, where the difference between sequential and independent design is shown. Third, the experimental results for both case studies are presented. Finally, some concluding remarks are given.

5.1 Case Studies

In this section, two different case studies are presented, i.e., two different disturbance signals consisting of multiple periods, to validate the developed theory. The reference trajectory of the carriage, presented in Section 2.1, is used. In which case, each print-pass corresponds to $N = 2999$ samples, i.e., ≈ 3 $[s]$, with the sampling time as $T_s = 0.001$ $[s]$. The experimental setup that is used, is without media handling. Meaning that the discrete marker measurements, as described in Section 2.1, are not available. This is why an external disturbance signal is created in the system to simulate the marker measurements. The two case studies describe the following situations.

Study 1: The first study has two contributions namely,

- it represents the actual reconstructed MPEs in the printing system, and
- the considered disturbance periods have a relatively small LCM, thus single-period RC can be used.

Study 2: The second study also has two contributions namely,

- potential benefits of the sequential design procedure are explored, since a higher frequency is used in the disturbance signal, and
- a relatively large LCM is obtained, to validate the application of multi-period RC.

In each case, the disturbance signal consists of two periodic signals, with period lengths given in Table 5.1.

Table 5.1: *Periods lengths in samples for each case study.*

	N_1	N_2	N_l
Case study 1	4499	11996	35988
Case study 2	477	11996	5722092

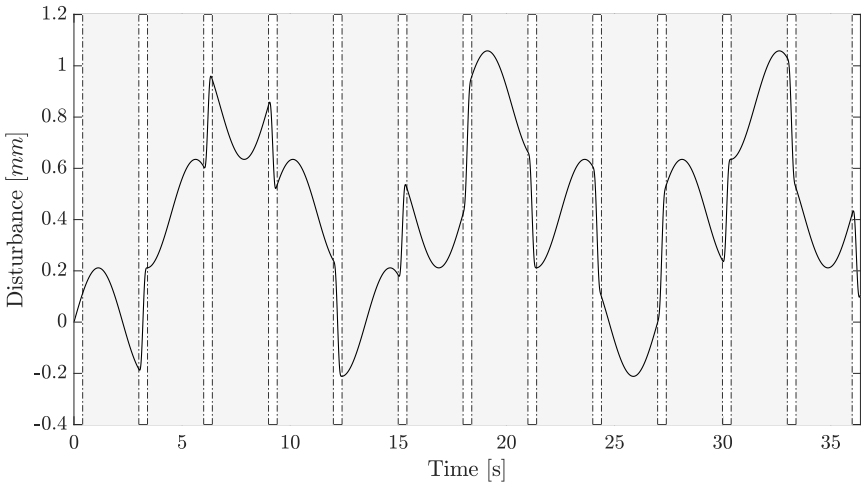

Figure 5.1: *Disturbance signal for case study 1. The grey areas indicate where the printing takes place.*

The disturbance signal for case study 1 is depicted in Figure 5.1, for 12 print-passes, i.e., ≈ 36 $[s]$. The grey areas indicate where the printing takes place, discussed in Section 2.1. As described in Section 2.1, the MPEs consists of multiple components, i.e., translation, rotation, and parabolic. The translation component is represented by a fourth-order step signal. This step consists of ≈ 0.5 $[mm]$ and period length $N_2 = 11996$ samples, i.e., periodic with 4 print-passes. It is deliberately chosen to be periodic with 4 print-passes for experimental time, although the real MPEs are periodic with ≈ 31 print-passes. The rotational and parabolic components are represented by a sine wave of period length $N_1 = 4499$ samples. The frequencies, normalized by each print-pass, are $\frac{1}{4}$ Hz and $\frac{2}{3}$ Hz respectively. Furthermore, this signal has an LCM of $N_l = 35988$ samples, i.e., 12 print-passes.

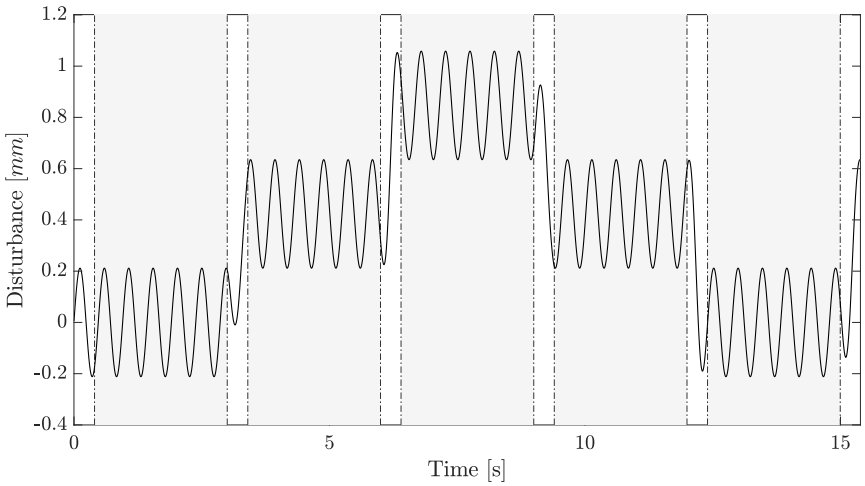

Figure 5.2: *Disturbance signal for case study 2. The grey areas indicate where the printing takes place.*

The disturbance signal for case study 2, depicted in Figure 5.2, is given for 5 print-passes, i.e., ≈ 15 $[s]$. The disturbance still consists of the translation component, with the same specifications as given above. However, the sine wave is chosen as $N_1 = 477$ samples, i.e., $\approx 2\pi$ Hz. The LCM is obtained as $N_l = 5722092$ samples, i.e., 1908 print-passes. Next, the multi-period RC designs are presented.

5.2 Multi-Period Repetitive Control Designs

In this section, the sequential design procedure, i.e., Procedure 4.1, is executed and compared with existing design results, e.g., [6, 16, 26], for case study 2. The following two cases are investigated.

- In Section 5.2.1, the sequential design procedure is executed for the cascaded and parallel structure, i.e., Procedure 4.1 for the RC control configuration in Figures 4.3 and 4.5. The objective is to illustrate the benefits of the cascaded structure with respect to robustness filter design. In this procedure, the learning gains are kept the same, i.e., $\alpha = 1$, as an initial design choice.
- In Section 5.2.2 the sequential design procedure for the parallel structure is compared with independent parallel design, see, e.g., [6, 16]. Now, Theorem 4.3 is combined with the sequential design procedure, to show that sequentially designing is potentially less conservative.

5.2.1 Sequential Design for Cascaded Structure and Parallel Structure

In this section, the sequential design procedure is followed step by step. The design conditions are visually displayed for the cascaded and parallel structures, to support the design choices. The resulting cut-off frequencies are depicted in Table 5.1. Every robustness filter is designed as a 50th order zero-phase low-pass FIR filter.

Table 5.1: *Cut-off frequencies for sequential cascaded and parallel design with* $\alpha = 1$.

	$f_{c,1}$ [Hz]	$f_{c,2}$ [Hz]
Sequential parallel design (Procedure 4.1)	35	0.1
Sequential cascaded design (Procedure 4.1)	35	45

1. The first step is designing the parametric model, i.e., $\hat{T}$, which is just the plant model $T(z)$, given in Section 2.3. Since $\hat{T}$ is non-minimum phase, the learning filter is obtained by stable inversion, i.e., ZPETC algorithm. Furthermore, the learning filter is kept the same for each individual repetitive controller in both structures, i.e., $L_1 = L_2$, as suggested in Section 4.5.1.

2. The second step is the loop-closing order. The choice of order can be influenced by a couple considerations.

   - The first consideration is the power corresponding to each disturbance frequency. If the contribution of one frequency and their harmonics is dominant, then possibly better performance can be achieved to start with closing this loop first.
   - The second consideration is starting with closing the loop with the largest disturbance frequency. This results in the fewer mismatches in the equivalent plant, meaning that the performance for the second loop is maintained.

   For the remaining of this design procedure, the latter consideration is used.

3. The next step is to design the robustness filters for each structure. The design steps for both structures are given simultaneously, however the differences are clearly depicted.

   In both structures, the first design problem is just single-period RC, with $T_0^{eq} = T$. By means of (4.19), the robustness filter can be designed, as depicted in Figure 5.3. Condition (4.19) is depicted with and without robustness filter and $\alpha = 1$ in this figure. Clearly, (4.19) is violated after ≈ 30 Hz, which means that the cut-off frequency of the first robustness filter, for both structures, is chosen as $f_{c,1} = 35$ Hz.

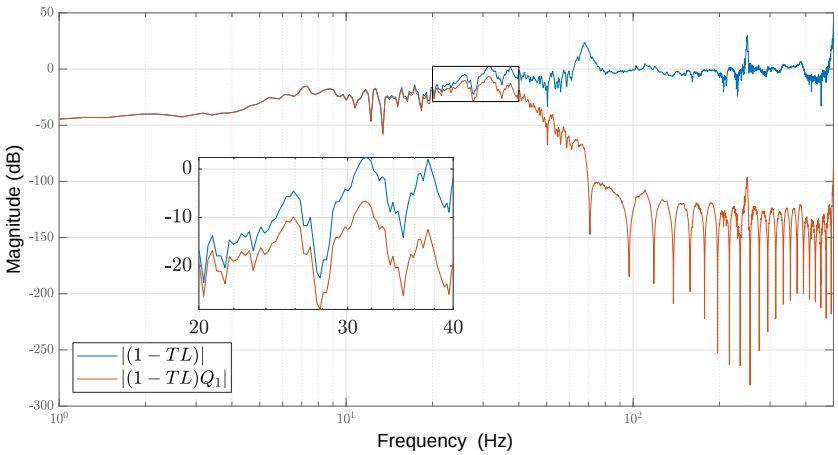

Figure 5.3: *Bode magnitude diagram for* (4.19)*, with and without the robustness filter.*

Next the equivalent plants, $T_{1,c}^{eq}$ for cascaded and $T_{1,p}^{eq}$ for parallel, are depicted in Figures 5.4 and 5.5 respectively.

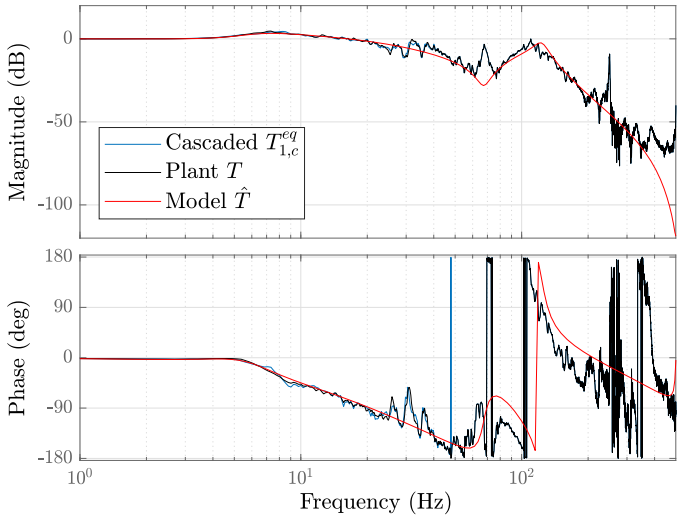

Figure 5.4: *Bode diagram of the plant T, the plant model $\hat{T}$, and the equivalent plant $T_{1,c}^{eq}$ for the cascaded structure.*

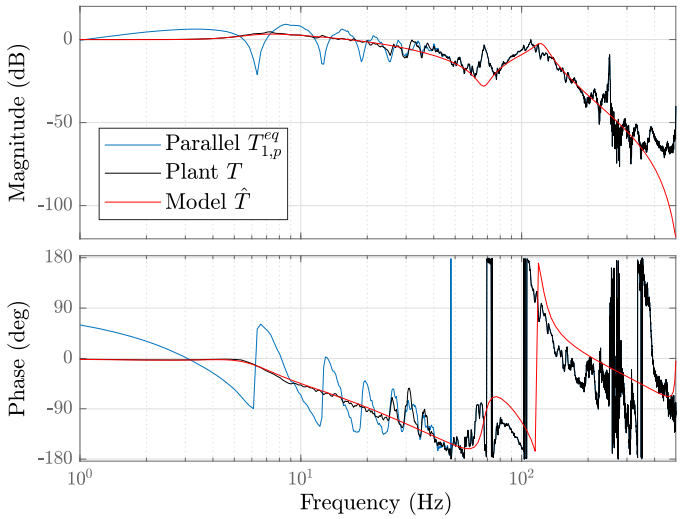

Figure 5.5: *Bode diagram of the plant T, the plant model $\hat{T}$, and the equivalent plant $T_{1,p}^{eq}$ for the parallel structure.*

The following observations are made with respect to the equivalent plants.

- The equivalent plant for the cascaded structure, depicted in Figure 5.4, is very similar to the original plant. The effect of including $\hat{T}$ is clearly visible, since no notches from the first repetitive controller are present. Before the cut-off frequency some minor mismatches are obtained, since $\hat{T} \neq T$, however this verifies that $L_2 = (T_{1,c}^{eq})^{-1}$ is unnecessary. Any mismatch can easily be encountered with the robustness filter design.
- Yet, the parallel structure shows much more mismatch before the cut-off frequency, depicted in Figure 5.5. In this case, the notches on $\approx 2\pi$ Hz and its higher harmonics, introduced by the first repetitive controller, are present in this equivalent plant, since they are not canceled

in (4.20). This is one of the reasons that it is not suitable to choose the second learning filter as $L_2 = (T_{1,p}^{eq})^{-1}$. Furthermore, amplification of intermediate frequencies is obtained, due to Bode's sensitivity integral. Thus, the robustness filter should encounter not only $\hat{T} \neq T$, but much more mismatch with respect to $L_2 \neq (T_{1,p}^{eq})^{-1}$.

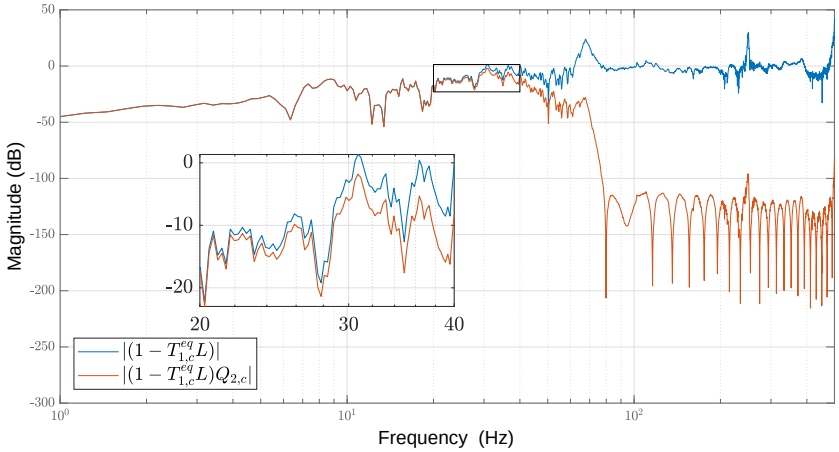

Figure 5.6: *Bode magnitude diagram for condition* (4.19)*, with and without the robustness filter for the cascaded structure.*

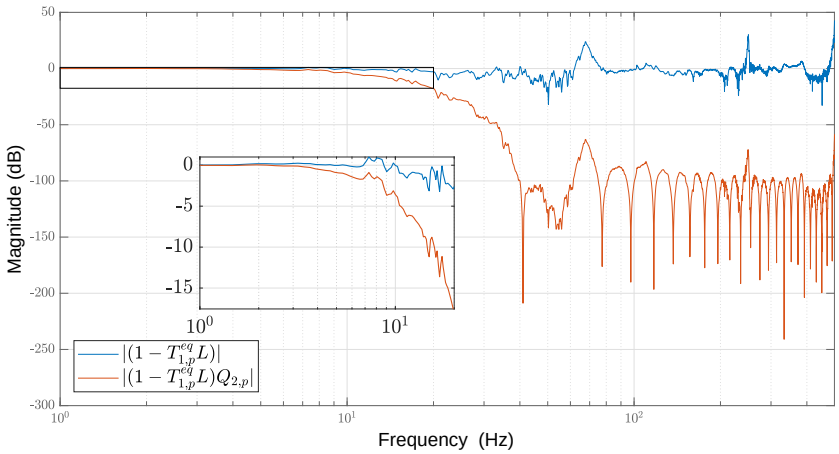

Figure 5.7: *Bode magnitude diagram for condition* (4.19)*, with and without the robustness filter for the parallel structure.*

Both equivalent plants are used in (4.19) to design the next robustness filter. This is depicted in Figures 5.6 and 5.7, with and without the second robustness filter, resulting in the following observations.

- In case of the cascaded structure, depicted in Figure 5.6, the first violation of (4.19) is still present at $\approx$ 30 Hz, as expected. However, due to the previous robustness filter, the cut-off frequency of this robustness filter can be increased to 45 Hz. This increases the performance in the second loop.

- Condition (4.19) for the parallel structure, depicted in Figure 5.7, is clearly different. The condition is already violated between $1-10$ Hz, due to the fact that $L_2 \neq (T_{1,p}^{eq})^{-1}$. Therefore, the cut-off frequency of the robustness filter should be chosen as $f_{c,2} = 0.1$ Hz, to satisfy (4.19). Implying no performance for the second loop.
- Alternatively, a band-pass filter might be used, to satisfy (4.19) in Figure 5.7. The band of the band-pass filter should be placed in the region where it will not violate (4.19), e.g., between 10 Hz and 20 Hz in Figure 5.7. Although (4.19) can be satisfied, it still restricts performance at lower frequencies. In case of the second case study, the second repetitive controller acts on $N_2 = 11996$ samples, i.e., $\frac{1}{4}$ Hz, thus minor/no performance will be obtained for the second loop.

From this design procedure, the following observations are made between the cascaded and parallel structure.

- Sequentially designing the robustness filters for the cascaded structure, results in a less conservative approach, since all preceding repetitive controllers are used in the design. The second cut-off frequency is increased, which results in more performance for the second loop. This is in contrast with an independent design approach, see, e.g., [26], where only one robustness filter for all loops would be designed based on $\hat{T}$, as discussed in Section 4.5.4. This results in less performance in subsequent loops. Hence, this illustrates the potential of sequential design with respect to the cascaded structure.
- The results indicate that sequential design for parallel structure is potentially very restrictive in the case $\alpha = 1$. The second cut-off frequency for a zero-phase low-pass filter is very low, implying no performance. A band-pass filter might be used, however this restrict the performance at lower frequencies as well.

Consequently, sequentially designing the cascaded structure has most favorable properties if $\alpha_i = 1 \, \forall i$. However, to compare the benefits of sequential parallel designs with existing parallel designs, the learning gains should satisfy Theorem 4.3, as suggested in [6, 16]. Combining this knowledge with the sequential design procedure is compared with the independent parallel design of [6, 16] in the next section.

5.2.2 Independent Design vs Sequential Design

Designing the filters and gains for the parallel structure, based on Theorem 4.3, is investigated next. First, the independent parallel design is shortly explained. Thereafter, the sequential parallel design procedure is executed.

All design results are depicted in Table 5.2. The learning gains are motivated by Theorem 4.3, i.e., $0 < \sum \alpha_i < 2$. The initial choice is $\sum \alpha_i = 1$, which means that the learning gains initial values are 0.5, for $n = 2$. The robustness filters are designed as a 50th order zero-phase low-pass FIR filter.

Table 5.2: *Cut-off frequencies and learning gains for the parallel structures.*

	$f_{c,1}$ [Hz]	$f_{c,2}$ [Hz]	$\alpha_{1,p}$	$\alpha_{2,p}$
Independent parallel design (Section 4.6.2)	55	55	0.5	0.5
Sequential parallel design (Procedure 4.1)	55	61	0.5	0.5

Independent parallel design is based on Procedure 3.1 with Theorem 4.3. In other words, the learning filters, robustness filters, and learning gains are all based on plant model $\hat{T}$, which results in the same filters and gains for each individual repetitive controller in the parallel structure. This design is similar to step 3, i.e., Figure 5.8, in the sequential design procedure, illustrated next. The resulting design choices are given in Table 5.2.

The sequential parallel design procedure is given in the following sequence of steps.

1. The same parametric model $\hat{T}$, i.e., $T(z)$ given in Section 2.1, and learning filter from Section 5.2.1 are used.
2. The same loop-closing order from Section 5.2.1 is used, i.e., starting with closing the loop for period length $N_1 = 477$ samples.
3. In Figure 5.8, condition (4.19) is depicted with and without robustness filter, and $\alpha_{1,p} = 0.5$. Violation is obtained at 60 Hz, meaning that the first cut-off frequency is obtained as $f_{c,1} = 55$ Hz. Notice that this cut-off frequency is 20 Hz higher than in Section 5.2.1. This already illustrates the influence of the learning gains, since a lower asymptotic error can be achieved with this cut-off frequency. However, this comes at the cost of convergence speed.

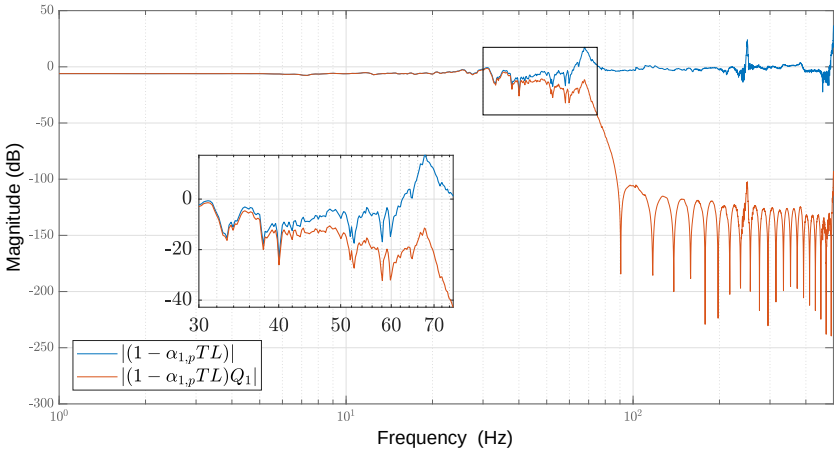

Figure 5.8: *Bode magnitude diagram for* (4.19)*, with and without the robustness filter, and* $\alpha_{1,p} = 0.5$.

By designing the robustness filter with $f_{c,1} = 55$, the following equivalent plant is obtained, depicted in Figure 5.9. Now, the notches at 2π Hz and their harmonics are present till 55 Hz. However, notice that amplification of intermediate frequencies is reduced with the learning gain as $\alpha_{1,p} = 0.5$. Using this equivalent plant in (4.19), results in Figure 5.10.

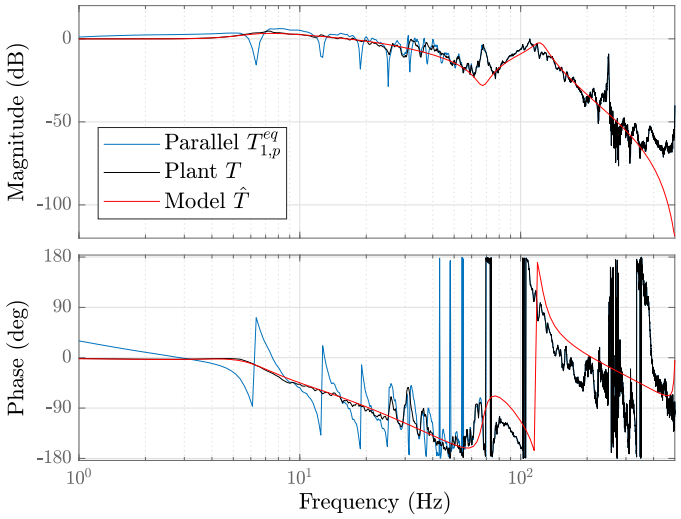

Figure 5.9: *Bode diagram of the plant T, the plant model $\hat{T}$, and the equivalent plant $T_{1,p}^{eq}$ for the parallel structure.*

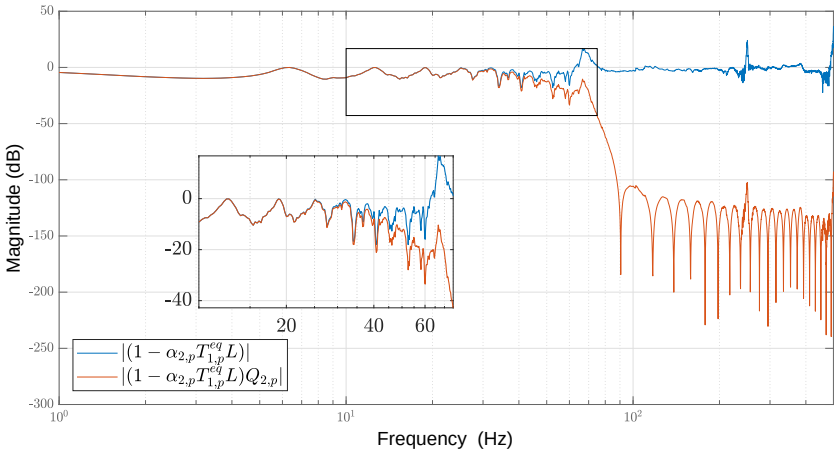

Figure 5.10: *Bode magnitude diagram for condition* (4.19)*, with and without the robustness filter for the parallel structure, and $\alpha_{2,p} = 0.5$.*

In sharp contrast with Figure 5.7, violation is obtained at $\approx$ 65 Hz. The first learning gain, i.e., $\alpha_{1,p} = 0.5$, causes reduction of intermediate frequencies in equivalent plant. Hence, the inverted notches in Figure 5.10 are no longer violating condition (4.19). This continues for the next equivalent plant, as long as Theorem 4.3 is satisfied. The second cut-off frequency is now designed as $f_{c,2} = 61$ Hz.

From these design procedures the following observations are made.

- In the independent parallel design, the filters and gains are all based on the model T, which results in the same filters and gains for each individual repetitive controller. This results in less performance of the total RC setup. In practice, each filter could be tuned for performance on experimental results, however this is unsatisfactory and time consuming.

- The sequential parallel design procedure, specifically designs for each individual repetitive controller, which results in a less conservative approach. Furthermore, specific increase in performance can be achieved with respect to the disturbances.
- In both designs, the achieved cut-off frequencies are higher than in the sequential parallel design of Section 5.2.1. This indicates the design freedom between the learning gain and robustness filter, i.e., between convergence speed and asymptotic error.

Consequently, the sequential parallel design is less conservative and results in improved performance with respect to independent parallel design.

Remark 5.1. The sequential design procedure is an iterative procedure. In practice, choosing some cut-off frequency deliberately lower for one loop, results in more performance in the next loop. For instance in Section 5.2.1, the first cut-off frequency could have been chosen higher, for instance 45 Hz. However, this influences the next robustness filter, to have a cut-off frequency less than 40 Hz, resulting in less performance in this loop. This also supports the importance of loop-closing order.

5.2.3 Concluding Remarks

In both sections, an illustration is given for the added value of the sequential design procedure for the parallel and cascaded structure. The following concluding remarks are applicable.

- The sequential design procedure for the cascaded structure can be used to design the robustness filters and learning gains. Modeling errors are included in the descriptions, meaning that the approach is less conservative.
- Sequentially design for the parallel structure can be achieved with prior knowledge on the learning gains, based on Theorem 4.3. Also for this structure it is less conservative than existing design results.
- In both designs, the number of individual repetitive controllers is $n = 2$. In theory, an unlimited number of individual repetitive controllers could be used and designed. However, notice that in the parallel structure the convergence speed becomes very restrictive if n increases, due to Theorem 4.3. This again shows the benefit of the cascaded structure for increasing n, since these learning gains are independent of n.

The design procedures are presented for the second case study, however similar steps are performed for the first case study. The final cut-off frequencies and learning gains that are used for experimental validation in both case studies are depicted in Table 5.3. The robustness filter is designed a as 50th order zero-phase low-pass FIR filter.

Table 5.3: *Cut-off frequencies and learning gains used for the experimental results.*

	$f_{c,1}$ [Hz]	$f_{c,2}$ [Hz]	$\alpha_{1,p}$	$\alpha_{2,p}$
Single-period RC (Procedure 3.1)	35	-	1	-
Sequential cascaded design (Procedure 4.1)	35	45	1	1
Sequential parallel design (Procedure 4.1)	55	61	0.5	0.5

5.3 Experimental Results

The tracking errors for both the case studies are given in this section. Single-period RC, parallel RC, and cascaded RC are implemented on the experimental setup, with Table 5.3 as the design choices. It is shown that each structure performs as expected. Yet, in both studies the cascaded structure has the most favorable results. The total experimental time for both case studies is 174 $[s]$, i.e., 58 print-passes.

5.3.1 Tracking Error: Study 1

In Figure 5.11, the tracking error for single-period RC, parallel RC, and cascaded RC is depicted, together with the external disturbance signal. In Figure 5.12, the zoom plot is depicted after 153 $[s]$, i.e., 51 print-passes. Single-period RC is implemented for the LCM of the disturbance signal, i.e., the period is $N_l = 35988$ samples. For the individual repetitive controllers in the parallel and cascaded structures, the period lengths $N_1 = 4499$ and $N_2 = 11996$ samples are used.

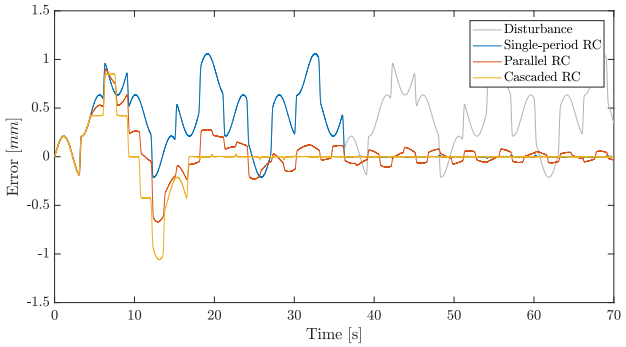

Figure 5.11: *Comparison of the disturbance, and the tracking error for single-period RC, parallel RC, and cascaded RC as function of time [s].*

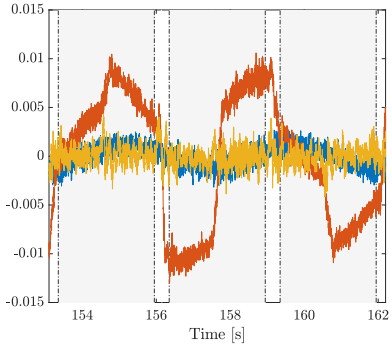

Figure 5.12: *Zoom plot the tracking error for single-period RC, parallel RC, and cascaded RC.*

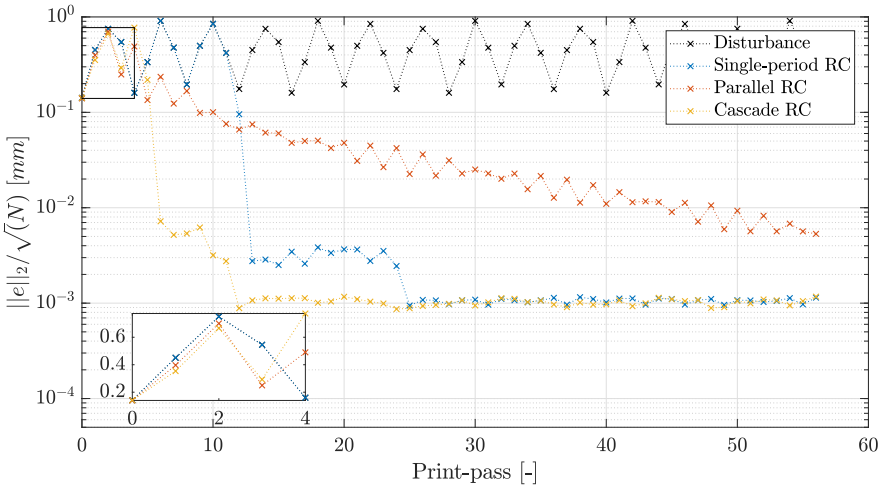

Figure 5.13: *Comparison of the normalized 2-norm over the print-passes, of the disturbance and the tracking error for single-period RC, parallel RC, and cascaded RC as function of print-passes. The zoom plot shows the early learning behavior of multi-period RC.*

The following observations from Figure 5.11 are made regarding the different structures.

- Single-period RC is (approximately) zero after 12 print-passes. However, it is likely that in many systems the LCM is not obtained within an acceptable time period. Hence, motivating multi-period RC.
- The parallel structure shows much interaction between the individual repetitive controllers, as illustrated in Section 4.7.4, resulting in slow convergence. Despite the fact that learning behavior

is obtained after 1.5 print-pass. The asymptotic tracking error is still not obtained after 154 $[s]$, depicted in Figure 5.12.

- The cascaded structure learns after 1.5 print-pass as well. It rejects the second period ($N_2 = 11996$) afterwards, implying (approximately) zero tracking error after $N_1 + N_2$ periods, i.e., 5.5 print-passes. In Figure 5.12, the resulting error only shows the remaining measurement noise.

In Figure 5.13 the normalized 2-norm is depicted for each structure. The error norm is normalized over one print-pass, i.e., $N = 2999$ samples. The following observations are made from this figure.

- Multi-period RC achieve earlier learning behavior, as depicted in the zoom plot of Figure 5.13.
- Due to the modeling error $\hat{T} \neq T$, cascaded RC and single-period RC, achieve the asymptotic error in two steps. Cascaded RC achieves the asymptotic error in 12 print-passes and single-period RC in 24 print-passes. Both reducing the error from $\mathcal{O}(10^0)$ to $\mathcal{O}(10^{-3})$.
- The parallel structure does not reach the asymptotic error within the experimental time. It reduced the error to $\mathcal{O}(10^{-2})$.

In Figure 5.14 the Power Spectral Density (PSD) for the disturbance and tracking error of the cascaded structure is depicted. The lower frequent range, including periods $N_1 = 4499$ and $N_2 = 11996$, are suppressed by the cascaded structure.

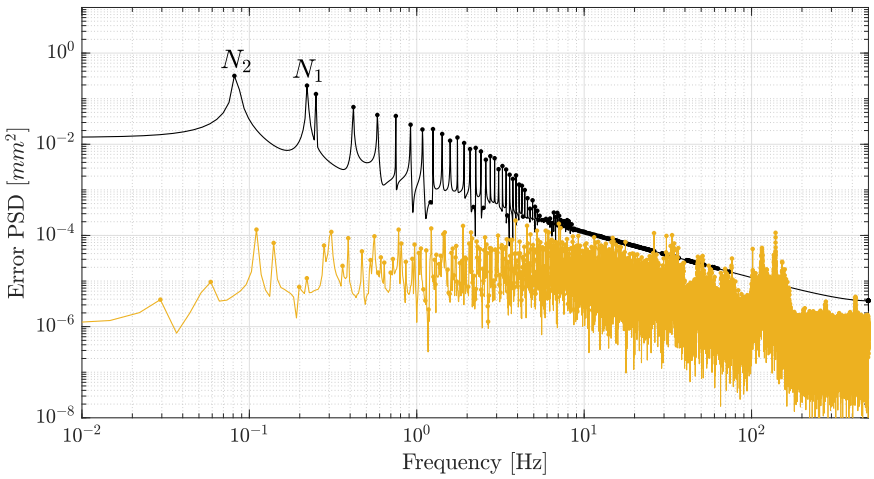

Figure 5.14: *Power Spectral Density (PSD) of the disturbance and tracking error of cascaded RC.*

5.3.2 Tracking Error: Study 2

In Figure 5.15, the tracking error of all RC structures is depicted, together with the disturbance signal. The corresponding zoom plot for the cascaded and parallel structure is depicted in Figure 5.16 after 123 $[s]$, i.e., 41 print-passes. The individual repetitive controllers for the cascaded and parallel structures are implemented for the period lengths $N_1 = 477$ and $N_2 = 11996$ samples. In this study, the single-period RC is implemented for the fourth-order step signal with period length $N_2 = 11996$ samples, since the LCM is $N_l = 5722092$ samples, i.e., 1908 print-passes. In practice, it is unrealistic to implement this LCM for single-period RC, since it requires a large memory space, and the speed of convergence is very slow, i.e., each repetitive update is 1908 print-passes.

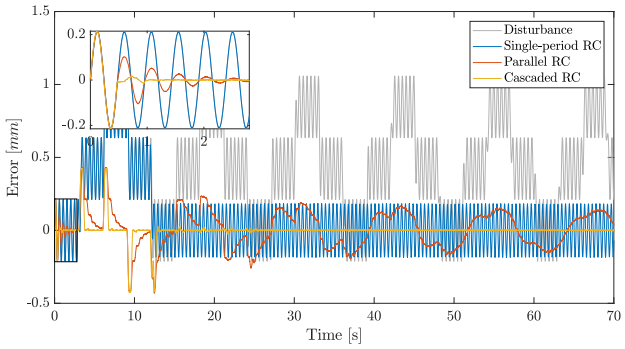

Figure 5.15: *Comparison of the disturbance, and the tracking error for single-period RC, parallel RC, and cascaded RC as function of time [s].*

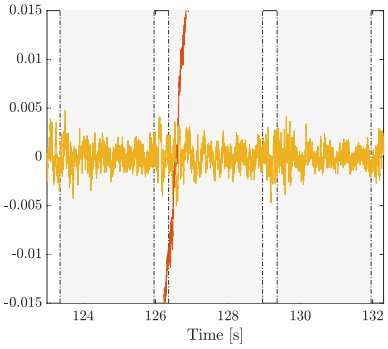

Figure 5.16: *Zoom plot the tracking error for parallel RC, and cascaded RC.*

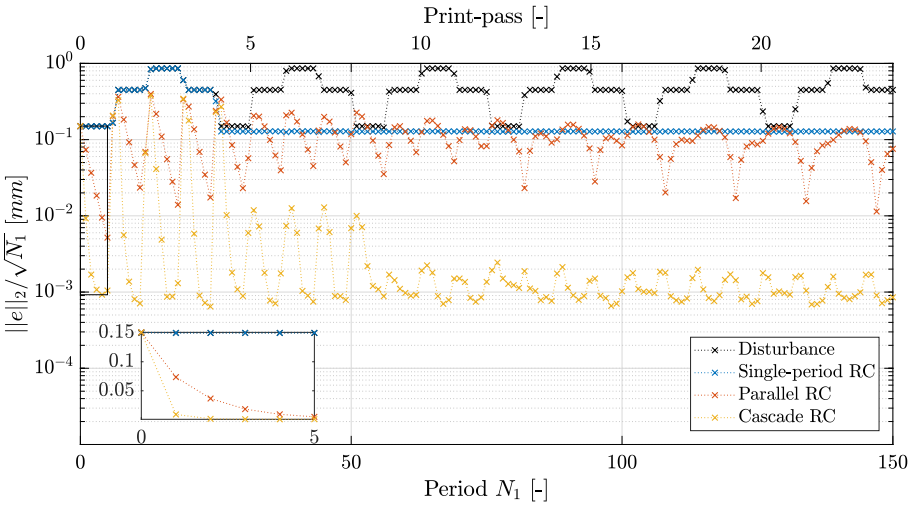

Figure 5.17: *Comparison of the normalized 2-norm, of the disturbance and the tracking error for single-period RC, parallel RC, and cascaded RC as function of the period N_1. The top x-axis show the corresponding print-passes. The zoom plot show the early learning behavior of multi-period RC.*

The following observation from Figure 5.15 can be made regarding the tracking error for each structure.

- First, single-period RC achieves disturbance rejection for period length $N_2 = 11996$ samples, i.e., after 4 print-passes. However, the remaining error ($\approx 2\pi$ Hz) cannot be perfectly rejected. This indicates the benefit of multiple memory loops.
- The parallel structure achieves fast learning, depicted in the zoom plot in Figure 5.15. It starts with reducing the disturbance frequency of $\approx 2\pi$ Hz after $N_1 = 477$ samples. Furthermore, the integrator action, i.e., 'shark teeth', is clearly visible. This results in slow convergence of the tracking error for the parallel structure, as described in Section 4.7.4.
- Fast learning is also achieved for the cascaded structure. Yet, the integrator action from the repetitive controller is also present here. However, the tracking error is (approximately) zero after $N_1 + N_2$ period lengths, due to $\hat{T}$ in the model structure. In Figure 5.16, only the measurement noise is left for the cascaded structure.

Remark 5.2. In case of single-period RC, the amplitude of the sine wave is still reduced. Although the sine wave is 'aperiodic' with the memory length, the repetitive controller still 'sees' the signal, meaning that it tries to reject it anyway.

The normalized 2-norm is depicted in Figure 5.17. In this case study, the normalization is done over the shortest period, i.e., $N_1 = 477$ samples, to demonstrate the fast learning behavior of multi-period RC. From this figure the following observations are made.

- Early learning behavior is achieved for multi-period RC. The convergence speed for rejecting the shortest period length $N_1 = 477$, is faster for cascaded RC then parallel RC, due to the learning gains, depicted in the zoom plot of Figure 5.16. However, both structures achieve the asymptotic error in the first few periods for this period length.
- Despite that, the overall tracking error norm achieves the asymptotic error in 52 periods, i.e., ≈ 25 $[s]$, for the cascaded structure. The parallel structure is not able to reach the asymptotic error within the experimental time.
- The errors are reduced from $\mathcal{O}(10^0)$ to, $\mathcal{O}(10^{-1})$ for single-period RC, $\mathcal{O}(10^{-2})$ for parallel RC, and $\mathcal{O}(10^{-3})$ for cascaded RC.

5.4 Concluding Remarks

Applying the theory to the wide-format RTR printing system and demonstrating the sequential design procedure, results in the following concluding remarks.

- The sequential design procedure is demonstrated for the cascaded and parallel structure and compared with existing independent designs. It can be shown that the sequential design procedure is less conservative in both structures in comparison with independent designs.
- Experimental validation is not executed for each different design for each structure. It can be concluded from the designs itself, that higher cut-off frequencies, with the same learning gains, achieve improved performance.
- The validation of the various RC structures showed that multi-period RC has favorable properties over single-period RC, especially the cascaded structure. Usually, the LCM is very high, which means that single-period RC is not suitable. Furthermore, the parallel structure showed much interaction between the individual repetitive controller, implying the benefit of including $\hat{T}$ in the model structure, i.e., cascaded RC. Notice that the convergence speed of the parallel structure is increased if the gap between the disturbance frequencies is lower.

Chapter 6

Conclusions and Recommendations

The research question of this thesis is defined as,

How to sequentially design multiple repetitive controllers to achieve rejection of periodically recurring medium positioning errors in wide-format roll-to-roll printing systems?

The following conclusions are based on the defined contributions in Section 1.5.

6.1 Conclusions

Characterization of repetitive medium positioning errors in wide-format roll-to-roll printing systems.

In Chapter 2, the Medium Positioning Errors (MPEs) are analyzed, and a detailed system description is presented. First, characterization of the repetitive MPEs showed three components coming from the Medium Positioning Roll (MPR), i.e., translational, rotational, and parabolic. These components consists of repetitive behavior, with the frequency corresponding to one full rotation of the MPR. Furthermore, the marker measurements showed more contributions to the MPEs from external disturbances, causing multiple components at higher frequencies. These components are reconstructed in a time-domain signal, and consequently used to track with the gantry-beam in the x-direction.

Development of a sequential design approach for multi-period RC.

The theory and design procedures for standard RC, given in Chapter 3, are extended towards multi-period RC in Chapter 4. Two multi-period RC structures are shown, i.e., the parallel and cascaded structure, where the cascaded structure showed most potential to reject exogenous disturbances with multiple unrelated periods. Analyses of the closed-loop system and stability revealed the potential for sequential design for RC. Subsequently, a sequential design approach is developed, with an explicit consecutive design procedure. It is shown that this procedure reduces conservatism and increases performance for both multi-period RC structures with respect to pre-existing design approaches.

Validation of the developed sequential design approach by means of simulation, using a parametric model of the gantry-beam in the x-direction.

Chapter 4 is concluded with simulation results for a parametric model of the gantry-beam in the x-direction. It is shown that the equivalent plant for the cascaded structure was very similar to the original plant, while the equivalent plant for the parallel structure clearly showed the influence of the preceding repetitive controllers. Furthermore, the simulations confirm the benefits of multiple repetitive controllers, since disturbance with multiple unrelated periods are rejected by both structures. The following conclusion from simulation results can be drawn for each RC framework regarding performance:

- Single-period RC showed slow convergence when the Least Common Multiple (LCM) of the disturbance periods is relatively high. Notice that this is usually the case in many systems, which may result in unacceptable performance.
- Parallel RC results in slow convergence due to interaction between the individual repetitive controllers.
- The convergence speed and asymptotic error of the cascaded structure showed the most potential.

Furthermore, an interaction analysis for both structures is performed, explaining the slow convergence of the parallel structure. This analysis concludes that the parametric model $\hat{T}$ assures reduction of interaction between the individual repetitive controllers if used in the control configuration, i.e., cascaded RC.

Experimental validation of the developed sequential design approach for multi-period RC on a wide-format roll-to-roll printing system.

Validation of the developed theory is presented in Chapter 5. The sequential design procedure is executed step by step to illustrate how to sequentially design repetitive controllers. The sequential design approach for the cascaded structure is compared with pre-existing results, showing that it is less conservative. The cut-off frequencies for the robustness filters and learning gains can explicitly be designed for modeling errors in the system description. This results in improved performance, i.e., lower asymptotic error. Pre-existing design approaches for the parallel structure showed the requirement to detune learning gains, resulting in slower convergence. However, sequentially designing the repetitive controllers in parallel with a prior knowledge on the learning gains, showed improved performance with respect to pre-existing results. Consequently, sequential design for both structures is less conservative and improves performance.

Experimental validation of a wide-format Roll-To-Roll (RTR) printing system is shown. Two cases studies are given to illustrate the potential of multi-period RC. It is demonstrated that single-period RC is not suitable if the LCM is too high. Furthermore, it is shown that the parallel structure results in slow convergence, despite the early learning behavior. To conclude, the cascaded structure showed superior results for rejecting disturbances with multiple unrelated frequencies, with respect to convergence speed, asymptotic performance, and early learning behavior. Other designs are not validated on the wide-format RTR printing system, since higher cut-off frequencies with similar learning gains implies improved performance.

6.2 Recommendations

The presented research gives rise to relevant future research directions, as discussed below.

6.2.1 Future Research

In this research, the potential of multi-period RC in frequency-domain is shown. Multi-period RC is able to reject disturbances with multiple unrelated periods, and all its higher harmonics. Alternatively, basis function can be used to reject specific periods only, as shown in [4, 20, 28]. This potentially reduces the interactions between repetitive controllers and results in faster convergence. However, some further research is required to include basis functions in multi-period RC.

- Stability should be guaranteed when including basis functions in the various structures. A lifting approach in frequency-domain is required, to prove stability. Some results are provided in [18], yet focuses mainly on stability analysis. Design for stability remains challenging.
- A more detailed analysis for various projection methods is required, e.g., (recursive) least squares, normalized least means squares, orthogonalized projection algorithm, ... , [9].

Furthermore, the interaction analysis for multi-period RC is shown in simulations. However, describing multi-period RC in time-domain, might result in a better view on the interactions between the individual

repetitive controllers. It is expected that these interactions are resulting from the transient behavior of each repetitive controller. Hence, time-domain descriptions might contribute to the theoretical analysis of these interactions.

All derivations and analyses are shown for Single-Input Single-Output (SISO). However, the developed theory might be extended to Multiple-Input Multiple-Output (MIMO). This enables to design each repetitive controller in multi-period RC for various degrees of freedom in many systems, as shown in [1].

Bibliography

[1] Blanken L., Hazelaar T., Koekebakker S., Oomen T., *Multivariable Repetitive Control Design Framework Applied to Flatbed Printing with Continous Media Flow.*. IEEE 56th Conference on Decision and Control (CDC), Melbourne, Australia, 2017.

[2] Blanken L., Willems J., Koekebakker S., and Oomen T., *Design techniques for multivariable ILC: Application to an industrial flatbed printer*, IFAC-PapersOnLine, vol. 49, no. 21, pp. 213 221, 7th IFAC Symposium on Mechatronic Systems, Loughborough, UK, 2016.

[3] Bolder J., Oomen, T., Koekebakker, S., and Steinbuch, M. *Using iterative learning control with basis functions to compensate medium deformation in a wide format inkjet printer.*, Mechatronics, 24(8), pp. 944-953, 2014.

[4] Bolk B., *LQ optimal lifted repetitive control with application to wide-format printing systems.*, Master's thesis, TU Eindhoven, 2017.

[5] Bristow D., Tharayil M., and Alleyne A., *A survey of iterative learning control: a learning-based method for high-performance tracking control.*, IEEE Control Systems Magazine, pp. 96-114, 2006.

[6] Chang W.S., Suh I.H., and Oh J.h., *Synthesis and analysis of digital multiple repetitive control systems.*, American Control Conference, Philadelphia, Pennsylvania, 1998.

[7] Desoer C., and Wang Y.T., *On the generalized Nyquist stability criterion*, IEEE Transactions on Automatic Control, vol. 25, no. 2, pp. 187196, April 1980.

[8] Francis B., and Wonham W., *The internal model principle of control theory*, Automatica, vol. 12, no. 5, pp. 457 465, 1976.

[9] Goodwin G.C., and Sin, K.S., *Adaptive Filtering Prediction and Control*, Prentice Hall, Englewood Cliffs, New Jersey, 1984.

[10] Hara S., Yamamoto Y., Omata T., and Nakano M., *Repetitive control system: a new type servo system for periodic exogenous signals*, IEEE Transactions on Automatic Control, vol. 33, no. 7, pp. 659668, 1988.

[11] Haslach H.W., *The moisture and rate-dependent mechanical properties of paper: A review*, Mechanics of Time-Dependent Materials, vol. 4, no. 3, pp. 169210, 2000.

[12] de Hoog T., *Stability and performance of memory loop filtered control systems.*, Literature survey. Delft university of technology, PATO, 1999.

[13] Hovd M., and Skogestad S., *Sequential design of decentralized controllers*, Automatica, vol. 30, no. 10, pp. 1601 1607, 1994.

[14] Longman R.W., Yeol J.W., and Ryu Y.S., *Improved methods to cancel multiple unrelated periodic disturbances by repetitive control.*, Advances in the Astronautical Sciences, Vol. 123, pp. 199-218, 2006.

[15] Longman R.W., *On the Theory and Design of Linear Repetitive Control Systems*, European Journal of Control, Vol. 16, no. 5, pp. 447-496, 2010.

[16] Lu W., Zhou K., and Wang D., *General parallel structure digital repetitive control.*, International Journal of Control, Vol. 86, No. 1, pp. 70-83, 2013.

[17] Mayne D.Q., *Sequential design of linear multivariable systems*, Electrical Engineers, Proceedings of the Institution of, vol. 126, no. 6, pp. 568572, 1979.

[18] Nagashima M., and Longman R.W., *Designing time invariant repetitive controllers using frequency raising of periodic coefficient projection algorithm.*, Journal of Aerospace Engineering, Vol. III, No. 1, 2011.

[19] Romme J.C.T., *Using ILC with basis functions to compensate periodic medium positioning errors in industrial wide-format printing systems.*, Masters thesis, TU Eindhoven, 2017.

[20] Shi Y., Longman R.W., and Nagashima M., *Small gain stability theory for matched basis function repetitive control.*, Acta Astronautica, vol. 95, pp. 260-271, 2014.

[21] Skogestad S., and Postlethwaite I., *Multivariable feedback control: analysis and design*, 2nd ed. Wiley, New York, 2005.

[22] Steinbuch M., *Repetitive control for systems with uncertain period time.*, Automatica, vol. 38, pp. 21032109, 2002.

[23] Steinbuch M., Weiland S., and Singh T., *Design of noise and period-time robust high-order repetitive control , with application to optical storage.*, Automatica, vol. 43, pp. 2086-2095, 2007.

[24] Teo Y., Fleming A., Eielsen A., and Tommy Gravdahl J., *A simplified method for discrete-time repetitive control using model-less finite impulse response filter inversion*, Journal of Dynamic Systems, Measurements, and Control, vol. 138, no. 8, pp. 081 0021081 00213, 2016.

[25] Tomizuka M., Tsao T.C., and Chew K.K., *Analysis and synthesis of discrete-time repetitive controllers*, Journal of Dynamic Systems, Measurements, and Control, vol. 111, p. 353, 1989.

[26] Winarto R., Koekebakker S., and Steinbuch M., *Combining ILC and repetitive control to handle repeating, event-triggered disturbances in precision inkjet printing.* American Control Conference, Chicago, IL, USA, 2015.

[27] Zapata P., Fransen M., ten Thije Boonkkamp J., and Saes L. *Heat and moisture transport in a paper sheet moving over a hot print surface.*, IEEE Communications Letters, vol. 17, 2012.

[28] Zwaans T.A.R., *Frequency variable repetitive control with basis functions with application to a professional printing system.*, Masters thesis, TU Eindhoven, 2014.

Appendix A

Derivation of Modifying Sensitivity for Cascaded Structure

A.1 Approach for n

Consider a multi-period RC control configuration, depicted in Figure A.1 on the left hand side, with the individual repetitive controllers as in (4.1) connected in the cascaded structure. For any number of n, this control problem can be transformed in a standard plant representation on the right hand side of Figure A.1.

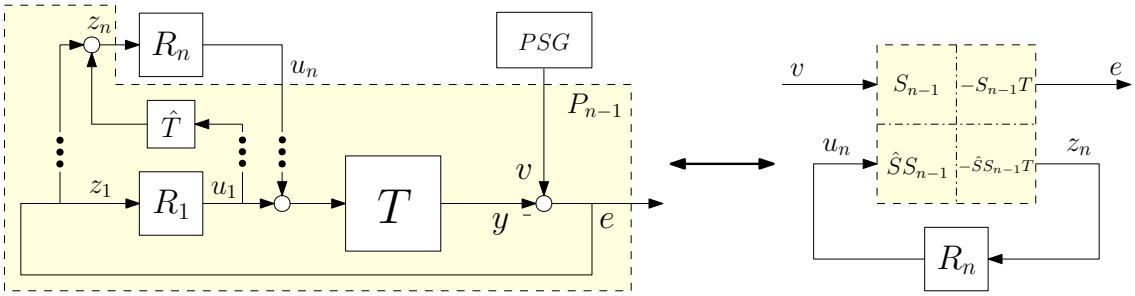

Figure A.1: *Left: Control configuration for multi-period RC in cascaded structure, Right: Standard plant representation. Note that the subscript $n-1$ holds for all variable S and $\hat{S}^{-1}$.*

The dotted yellow block, depicted by P_{n-1}, is the transformation matrix between the defined in- and outputs of the standard plant. The defined inputs are, the disturbance v and output of the repetitive controllers u_n. The outputs are, the error signal e and the input z_n for the repetitive controller.

Let the error propagation $e = v - y$, and the input for the repetitive controller z_n be given by,

$$e = \underbrace{\prod_{i}^{n-1}[(1+T_{i-1}^{eq}R_i)^{-1}]}_{S_{n-1}} v - \prod_{i}^{n-1}[(1+T_{i-1}^{eq}R_i)^{-1}]Tu_n, \tag{A.1}$$

$$z_n = \underbrace{\prod_{i}^{n-1}[(1+\hat{T}R_i)]\prod_{i}^{n-1}[(1+T_{i-1}^{eq}R_i)^{-1}]}_{\hat{S}_{n-1}^{-1}S_{n-1}} v - \prod_{i}^{n-1}[(1+\hat{T}R_i)]\prod_{i}^{n-1}[(1+T_{i-1}^{eq}R_i)^{-1}]Tu_n. \tag{A.2}$$

Equation A.1 and A.2 are written in a general format. So that for any number n, the equations describe the right in- and outputs of the standard plant P_{n-1}.

The control objective of the standard plant, is to design the repetitive controller R_n for any n, such that the closed-loop system is stable. The closed-loop transfer from v to e is obtained by the lower Linear Fractional Transformation (LFT),

$$F_l(P_{n-1}, R_n) = S_{n-1} - S_{n-1}TR_n(1 + \hat{S}_{n-1}^{-1}S_{n-1}TR_n)^{-1}\hat{S}_{n-1}^{-1}S_{n-1}, \tag{A.3}$$

$$= S_{n-1}(1 + \underbrace{\hat{S}_{n-1}^{-1}S_{n-1}T}_{T_{n-1}^{eq}}R_n)^{-1}, \tag{A.4}$$

which is the modifying sensitivity function with all loops closed. Two observations are made,

- first the resulting function (A.4) is the product of sensitivities for each repetitive controller.
- Second, it is clearly visible that each next connected repetitive controller R_n see a different 'plant to be controlled', called the equivalent plant.

This equivalent plant is basically the transfer function from u_n to z_n, which is obtained as,

$$T_{n-1}^{eq} = \hat{S}_{n-1}^{-1}S_{n-1}T. \tag{A.5}$$

This equivalent plant can be written dependent on the previously equivalent plant, i.e., in a recursive form,

$$T_i^{eq} = (1 + T_{i-1}^{eq}R_i)^{-1}T_{i-1}^{eq}(1 + \hat{T}R_i), \tag{A.6}$$

for $i = 1, 2, ..., n-1$.

Remark A.1. If $\hat{T} = T$ then $T_{n-1}^{eq} = T \,\forall\, n$, since $\hat{S}^{-1}$ and S cancel.

Technische Universiteit
Eindhoven
University of Technology

Declaration concerning the TU/e Code of Scientific Conduct for the Master's thesis

I have read the TU/e Code of Scientific Conduct[i].

I hereby declare that my Master's thesis has been carried out in accordance with the rules of the TU/e Code of Scientific Conduct

Date

03-12-2018

Name

Patrick Bevers

ID-number

0858003

Signature

Submit the signed declaration to the student administration of your department.

[i] See: http://www.tue.nl/en/university/about-the-university/integrity/scientific-integrity/
The Netherlands Code of Conduct for Academic Practice of the VSNU can be found here also.
More information about scientific integrity is published on the websites of TU/e and VSNU